

1 **Title**

2 **Counteracting Genome Instability by p53-dependent Mitosis**

3
4 **Authors**

5 Jianqing Liang^{1,6#}, Zubiao Niu^{1#}, Xiaochen Yu^{1#}, Bo Zhang^{1,2}, Manna Wang^{1,4}, Banzhan Ruan¹,
6 Hongquan Qin^{1,4}, Xin Zhang¹, You Zheng¹, Songzhi Gu¹, Xiaoyong Sai³, Yanhong Tai⁵, Lihua
7 Gao¹, Li Ma⁴, Zhaolie Chen¹, Hongyan Huang^{2*}, Xiaoning Wang^{3*}, Qiang Sun^{1*}

8
9 **Affiliations**

10 ¹Laboratory of Cell Engineering, Institute of Biotechnology, 20 Dongda Street, Beijing 100071, P.R.
11 China.

12 ²Department of Oncology, Beijing Shijitan Hospital of Capital Medical University, 10 TIEYI Road,
13 Beijing 100038, P. R. China;

14 ³National Clinic Center of Geriatric & the State Key Laboratory of Kidney, the Chinese PLA General
15 Hospital, Beijing 100853, P.R.China

16 ⁴Institute of Molecular Immunology, Southern Medical University, Guangzhou 510515, P. R. China

17 ⁵The 307 Hospital, 8 Dongda Street, Beijing 100071, P. R. China

18 ⁶State Key Laboratory of Genetic Engineering, School of Life Science, Human Phenome Institute,
19 Fudan University, Shanghai, 200438, People's Republic of China.

20
21 *Correspondence to:

22 **Qiang Sun**

23 Email: sunq@bmi.ac.cn

24 **Xiaoning Wang**

25 Email: xnwang88@163.com

26 **Hongyan Huang**

27 Email: hhongy1999@126.com

28
29 # These authors contributed equally to this work

30

31

32 **Abstract**

33 Entosis was proposed to promote aneuploidy and genome instability by cell-in-cell mediated
34 engulfment in tumor cells. We reported here, in non-transformed epithelial cells, that entosis
35 coupled with mitotic arrest functions to counteract genome instability by targeting aneuploid mitotic
36 progenies for engulfment and elimination. We found that the formation of cell-in-cell structures
37 associated with prolonged mitosis, which was sufficient to induce entosis. This process was
38 controlled by the tumor suppressor p53 (wild type) that upregulates Rnd3 expression in response to
39 DNA damages associated with prolonged metaphase. Rnd3 compartmentalized RhoA activities
40 accumulated during prolonged metaphase to drive cell-in-cell formation. Remarkably, this
41 prolonged mitosis-induced entosis (mintosis) selectively targets non-diploid progenies for
42 internalization, blockade of which increased aneuploidy. Thus, our work uncovered a heretofore
43 unrecognized mechanism of mitotic surveillance for entosis, which eliminates newly-born abnormal
44 daughter cells in a p53-depedent way to maintain genome integrity.

45 **Key Words:** mintosis, entosis, mitosis, cell-in-cell, p53, RND3, mitotic surveillance

46

47

48 **MAIN TEXT**

49 **Introduction**

50 Cell division via mitosis is strictly regulated to ensure the production of healthy daughter
51 cells. During mitosis, correct segregation and distribution of genetic materials into daughter cells
52 rely on proper activation of spindle assemble checkpoint (SAC) (Musacchio, 2015; Sivakumar &
53 Gorbsky, 2015). SAC is activated by unsatisfied microtubule-kinetochore attachment, leading to the
54 recruitment of SAC proteins MAD2, BUBR1 and BUB3 together with CDC20 (Kapanidou et al,
55 2017) to kinetochores to form mitotic checkpoint complex (MCC). MCC functions to inhibit
56 anaphase-promoting complex or cyclosome (APC/C), the multisubunit E3 ubiquitin ligase essential
57 for metaphase-anaphase transition in the presence of CDC20. Molecules disrupting MCC such as
58 CUEDC2 could activate APC/C via preventing MAD2 from binding to CDC20 (Gao et al, 2011).
59 Activated APC/C promotes proteasome-dependent degradation of cyclin B1 (CCNB1) to allow
60 mitotic exit, and securin to release separase (ESPL1) which leads to cohesion destruction and
61 subsequent sister chromatid separation (Musacchio, 2015; Sivakumar & Gorbsky, 2015). Prolonged
62 SAC activation due to mitotic aberrations generally leads to mitotic arrest and often, but not always,
63 to mitotic catastrophe (specifically referred to catastrophic death here) (Vitale et al, 2011). Those
64 that eventually pass mitotic arrest are prone to produce aneuploid/polyploid (non-diploid) daughter
65 cells that need to be dealt with post-mitotically, otherwise impair tissue homeostasis and/or
66 contribute to tumorigenesis (Funk et al, 2016; Santaguida & Amon, 2015).

67 Entosis is a recently defined non-apoptotic cell death program, where suspended epithelial
68 cells actively penetrate into and die inside of their neighbors (Overholtzer et al, 2007). Cell
69 penetration leads to the formation of so called “cell-in-cell” structures (CIC), which requires
70 polarized actomyosin contraction at the rear cortex of the internalizing cells. The polarized
71 distribution of actomyosin is established by local inhibition of RhoA-ROCK signaling at cell-cell
72 junctions, where lie junction-associated inhibitors, such as p190A RhoGAP (Sun et al, 2014a).

73 Multiple factors, including CDKN2A (Liang et al, 2018), IL-8 (Ruan et al, 2018a) and membrane
74 cholesterol and lipids (Ruan et al, 2018b), that affects RhoA signaling were recently identified as
75 important regulators of entotic CIC formation. Although initially viable, majority of the internalized
76 cells die non-autonomously with the assistance of outer host cells (Florey et al, 2011). Pathologically
77 in the context of tumors, entosis was proposed as a cellular mechanism of cell competition that
78 selects winner tumor cell clones via internalizing and killing loser cells (Kroemer & Perfettini, 2014;
79 Sun et al, 2014b), and promotes tumor evolution by inducing genome instability of outer cells
80 (Krajcovic et al, 2011; Mackay et al, 2018). However, its roles in physiological context remain
81 largely speculative and mysterious up to date.

82 The tumor suppressor p53 was known as “guardian of genome”. In responding to acute DNA
83 damages, signaling cascades involving ATM/ATR and/or CHK1/CHK2 were initiated to activate
84 p53, which was believed to triggers cellular responses such as cell cycle arrest or apoptosis to
85 counteract the genotoxic stresses (Biegging et al, 2014). p53 initiates different cellular responses
86 generally via regulating expression of specific downstream target genes, such as the CDK inhibitor
87 *p21* for cell cycle arrest and the pro-apoptotic Bcl-2 family members *Puma* and *Noxa* for apoptosis
88 (Joerger & Fersht, 2016). While cell cycle arrest was envisaged to provide cells an opportunity to
89 fix the repairable DNA damages before next round of cell cycle and thus prevent propagation of
90 potentially harmful mutations, cell death by apoptosis was likely a more aggressive and efficient
91 way to eliminate cells harboring more severe genetic aberrations, and thereby to maintain genome
92 integrity (Biegging et al, 2014; Joerger & Fersht, 2016). In addition to apoptosis, p53 was also
93 implicated in other forms of cell deaths that play roles in removing cells with DNA damages
94 (Kruiswijk et al, 2015). Mitotic catastrophe was believed to be a p53-regulated non-apoptotic cell
95 death that eliminates questionable cells during prolonged mitosis which generally takes place with
96 DNA damages (Ranjan & Iwakuma, 2016). Nevertheless, it’s unknown whether genetically

97 questionable progenies following mitosis were actively removed by a non-apoptotic cell death that
98 might also be regulated by p53.

99 Here, we demonstrate that p53 mediates the internalization and elimination of aneuploidy
100 daughter cells from transient mitotic arrest by a non-apoptotic death program termed mitosis
101 (derived from prolonged mitosis-induced entosis), which was driven by Rnd3-compartmentalized
102 RhoA activities in daughter cells that were internalized in response to DNA damages during
103 prolonged metaphase. Thus, our work identified a novel surveillance mechanism for entosis, in a
104 wild type p53-dependent way, to safeguard mitosis and genome integrity.

105 **Results**

106 **Entosis is Associated with Prolonged Mitosis**

107 In a process of tracking entotic CIC formation by time lapse microscopy in adherent
108 MCF10A, a non-transformed human mammary epithelial cell line routinely used for entosis
109 research, we unexpectedly found that majority (22/24) of CIC structures formed shortly after mitotic
110 cell division, in spite of a few of exceptions where one adherent cell migrating into and one
111 suspended cells sinking into their neighbors (Fig. 1A, C and Movie S1). Once internalized, the inner
112 cells readily underwent cell death (Fig. 1B, D, Fig. S2 and Movie S2-3) as previously reported for
113 entosis (Overholtzer et al, 2007). The result suggests that mitosis could initiate entosis in adherent
114 monolayers as recently reported for the induced entosis, via CDC42 depletion, in 16HBE cells
115 (Durgan et al, 2017). However, only a small portion of the mitotic events (<0.5% or so) led to entosis
116 in normal adherent MCF10A culture, suggesting that entotic mitosis, referring to mitosis leading to
117 entosis, is intrinsically different from normal mitosis. Comparison analysis revealed a significantly
118 prolonged metaphase in entotic mitosis of MCF10A (Fig. 1A, 1E and Movie S1, 2), indicating that
119 entosis may occur in respond to mitotic arrest.

120 **Transient Mitotic Arrest Activates Entotic CIC Formation**

121 To test this idea, we performed RNAi-mediated knockdown (KD) of CDC20 (Figure 2A)
122 and ESPL1 (Figure S3A), two core genes critical for metaphase to anaphase transition, in MCF10A
123 cells. Both CDC20 and ESPL1 depletion efficiently induced mitotic arrest of various extents (Figure
124 2B and S3B-C) and importantly increased CIC formation 36 hours post siRNA transfection (Figure
125 2C and S3D) when a number of mitotically arrested cells started to appear. Similar to that in
126 spontaneous entosis, mitosis is corresponding to majority of CIC formation (47/51 for CDC20 KD,
127 53/54 for ESPL1 KD) for these two induced entosis (Figure 2D and S3E), consistent with which,
128 blocking cell cycle with CDKs' inhibitors (Ro-3306 and SU-9516) efficiently inhibited CIC
129 formation (Figure 2C). Interestingly, while metaphase of normal division peaks around 20 min for
130 MCF10A cells (Figure 2B, 2E and S3C), entotic mitosis displays a restricted metaphase range from
131 30 min to 195 min (Figure 2E and S3C) with most entotic events preceded by mitotic arrest of 60
132 min or so. Mitotic cells arrested for more than 200 min were unlikely capable of division and
133 eventually ended up with catastrophic death (Figure 2E, 2F, S3C and Movie S4). Therefore, mitotic
134 catastrophe and entosis are likely cooperated to safeguard aberrant mitosis with each of them worked
135 before and after mitosis, respectively. To further confirm the role of mitotic arrest in activating
136 entosis, mitotic arrest induced by depleting CUEDC2, a promoter of metaphase-anaphase transition
137 (Gao et al, 2011), was released by co-depleting either BUBR1 or MAD2 (Figure 2G and S3F-H),
138 two essential components of mitotic checkpoint complex (Sivakumar & Gorbsky, 2015). As a result,
139 mitosis-activated CIC formation induced by CUEDC2 depletion was inhibited as well (Figure 2H-
140 I). Together, the data presented above supports that mitotic arrest, indicated by prolonged metaphase,
141 primes cells to undergo entotic CIC formation post-mitotically. To differentiate from entosis
142 induced via other ways, we refer to this prolonged mitosis-induced entosis as mintosis hereafter.

143 **DNA Damages Promote Mintosis**

144 DNA damages were reported being associated with prolonged mitosis (Ganem & Pellman,
145 2012). We therefore hypothesized that DNA damages might account for mintosis incurred by

146 prolonged mitosis. Consistent with this idea, time lapse-associated immunostaining indicated that
147 cells of longer metaphase were positive in γ H2AX (Figure 3A-B, Figure S4A), a marker of DNA
148 damages, with nuclear γ H2AX foci significantly more than those in cells of shorter metaphase
149 (Figure 3C). Moreover, the nuclear γ H2AX foci were correlated with formation of mitotic CIC
150 structures, where the internalizing mitotic daughter cells contained more nuclear γ H2AX foci than
151 their siblings that didn't form CIC structures (Figure 3D). Significantly, mitotic CIC formation
152 was suppressed by γ H2AX depletion (Figure 3E-F) or inhibition of its downstream signaling by
153 chemical compounds (Figure 3G) or siRNAs targeting ATM, ATR, CHK1 and CHK2 (Figure S4B-
154 C), indicating essential role of DNA damage signaling in mitosis. To directly examine the effects
155 of DNA damages on mitosis, cells synchronized in M phase were treated with mitomycin, a DNA
156 damage inducer that causes double strand break, and then cultured in normal media to allow mitotic
157 exit and cytokinesis. As shown Figure 3H-I, mitomycin treatment efficiently activated DNA damage
158 response, indicated by enhanced expression of γ H2AX and phosphorylated ATM (Figure 3H), and
159 significantly increased mitotic CIC formation following cell division (Figure 3I). These effects
160 were confirmed by bleomycin, another DNA damage inducer (data not shown). Interestingly, DNA
161 damage signaling was likely also activated in human breast cancer tissues with high CIC structures,
162 where nuclear γ H2AX foci were significantly more than those in low CIC breast cancer tissues
163 (Figure 3J-K). Together, these data suggest that prolonged mitosis-associated DNA damages induce
164 mitosis.

165 **P53 is Required for Daughter Cells to Undergo Mitosis**

166 Since p53 is the key mediator of DNA damage signaling, we then explore the involvement
167 of p53 in mitosis. Time lapse-associated immunostaining indicated that high level of p53
168 accumulated in the nuclei of daughter cells penetrating into their neighbors (Figure 4A). The
169 expression levels of p53 were positively correlated with γ H2AX foci formation (Figure 4B), and
170 higher in mitotic cells of longer metaphase (Figure 4C), and higher in the internalizing daughter

171 cells as compared with their non-mintotic sibling cells (Figure 4D) and those from normal division
172 (Figure 4E). Importantly, RNA interference-mediated knockdown of p53 significantly suppressed
173 mintotic CIC formation induced by CDC20 or CUEDC2 knockdown (Figure 4F-G), suggesting that
174 p53 is required for mintosis. p53 likely functions primarily in the mitotic daughter cells that
175 penetrate into their neighbors, as p53 knockdown reduced the frequency of cells' penetration as
176 inners when co-cultured with control cells (Figure 4H-J). Thus, p53 is likely a key regulator of
177 mintosis.

178 **RhoA Activity Accumulated with Prolonged Metaphase Promotes Mintosis**

179 To explore the potential mechanisms underlying the regulation of mintosis by p53, we first
180 examine changes in RhoA activities, which is prerequisite for CIC formation (Ning et al, 2015; Sun
181 et al, 2014a) and regulated by p53 signaling (Gadea et al, 2007; Xia & Land, 2007), during mintosis.
182 CDC20-depleted cells were stained with antibody for p-MLC, a readout of RhoA activities,
183 following 4-hour time lapse microscopy (Movie S5). As shown in Figure 5A-C, mitotic cells of
184 longer metaphase tended to display higher p-MLC intensity, in agreement with which, RhoA
185 activities in mitotic cells did accumulate over time as monitored by FRET time lapse analysis
186 (Figure 5D, S5A-B and Movie S6). Since mintotic CIC formation occurred in daughter cells, we
187 examined whether enhanced RhoA activities in mother cells could be inherited by daughter cells.
188 RhoA activities of daughter cells right after cytokinesis were compared with those of their respective
189 mother cells in the end of metaphase by FRET time lapse. As shown in Figure S5A-D, the two
190 sibling daughter cells are tightly adherent to their mothers in RhoA activities, which is true for both
191 normal and mintotic cell division, suggesting that RhoA activities could be transmitted from mother
192 cells to daughters with little loss. We then examined the effects of changed RhoA activities on
193 mintotic CIC formation, consistent with essential role of RhoA in entosis, ectopic overexpression
194 of RhoA significantly increased mintotic CIC frequency (Figure 5E), and inhibition of RhoA

195 signaling by Y27632 targeting ROCKs efficiently suppressed mitotic CIC formation (Figure 5F),
196 supporting a role of increased RhoA activity in promoting mitosis.

197 **p53-regulated Rnd3 is Essential for Compartmentalizing RhoA Activities and Mitosis**

198 Since polarized distribution of actomyosin, the downstream effector of RhoA signaling, is
199 essential for cells' penetration into their neighboring cells (Sun et al, 2014a), we examined the
200 expression of p-MLC, the readout of contractile actomyosin and RhoA activity, in the intermediate
201 mitotic CIC structures. As shown in Figure 5G and S5E, p-MLC displays typical asymmetric
202 distribution pattern, characterized by higher intensity at the rear cortex than that at cell-cell junctions
203 marked by E-cadherin where RhoA activities were actively suppressed by inhibitors such as p190A
204 RhoGAP (Sun et al, 2014a). While wild type p53 was known to negatively regulate RhoA signaling
205 through its downstream target Rnd3 (Ongusaha et al, 2006; Zhu et al, 2014), an atypical Rho GTPase
206 that inhibits RhoA signaling by directly targeting ROCK I (Ongusaha et al, 2006; Riento et al, 2003)
207 and p190A RhoGAP (Wennerberg et al, 2003). We therefore hypothesized that Rnd3 may facilitate
208 CIC formation via helping compartmentalize RhoA activities. In agreement with this notion, Rnd3,
209 regulated by p53 (Figure S5F), specifically localizes at cell-cell junctions while MLC is enriched at
210 the cortical periphery away from junctions during CIC formation (Figure 5H). SiRNA-mediated
211 Knockdown of Rnd3 led to increased pMLC staining at cell-cell junctions (Figure 5I-J and S5G),
212 suggesting that the junctional-localization of Rnd3 spatially restricts RhoA pathway activity and
213 inhibits myosin contraction at cell-cell junctions, which promotes CIC formation. Consequently,
214 Rnd3 depletion significantly inhibited both mitotic and mitotic CIC formation (Figure 5K-L).
215 Together, the above data fits a model whereby p53-regulated Rnd3 compartmentalizes RhoA
216 activity in daughter cells from prolonged mitosis to drive CIC formation.

217 **Mitosis Selectively Targets Mitotic Progenies of Non-Diploidy**

218 Prolonged metaphase due to SAC activation allows cells to fix problems during chromosome
219 segregation. Nevertheless, prolonged mitosis also elicit structural DNA damages (Dalton et al, 2007;
220 Ganem & Pellman, 2012) that, via truncated DNA damage response (DDR), induce whole-
221 chromosome missegregation (Bakhoun et al, 2014), leading to non-diploid daughter cells
222 (Bakhoun et al, 2017). We therefore hypothesized that mintosis was set to ensure selective
223 elimination of those non-diploid cells. Fluorescent in situ hybridization (FISH) was employed to
224 access ploidy changes in MCF10A cells plated on gridded-glass bottom dish following 24 hour-
225 time lapse microscopy, and the metaphase and position histories of target cells were determined by
226 retroactive review of the time lapse records (Movie S7). While mitosis of short metaphase, based
227 on the probes used, generally gave rise to diploid progenies (96.9%) (Figure 6A and 6C), cells of
228 prolonged metaphase penetrating their neighbors to form CIC structures were largely non-diploid
229 (50.7%) (Figure 6B, 6D and S6A). This non-diploid rate of mitotic inner cells is similar to that
230 (43.9%) of inner cells of pre-existing CIC structures (Figure 6E), consistent with our observation
231 that majority of CIC structures were from prolonged mitosis. Intriguingly, the sibling cells that did
232 not participate into CIC formation were largely diploid (88.5%) (Figure 6F) in a rate similar to the
233 whole MCF10A population (89.9%) (Figure 6G). And a small portion of inner cells that eventually
234 got released from CIC structures were also largely diploid (83.8%) (Figure 6H and Figure S6B).
235 Therefore, mintosis selectively targets non-diploid daughter cells for elimination, which may play
236 an essential role in maintaining population genetic integrity, as blocking mintosis by Y27632, an
237 inhibitor of ROCK kinases prerequisite for CIC formation (Sun et al, 2014b), significantly increased
238 non-diploid cells in the cell population (Figure 6I). Thus, our data support that p53-regulated
239 mintosis may serve as a cellular mechanism of mitotic surveillance.

240 **Discussion**

241 In summary, we proposed a CIC-mediated mechanism of post-mitotic surveillance as
242 mintosis whereby non-diploid progenies from prolonged mitosis were eliminated in a p53-

243 dependent manner. In this model (Figure S1), γ H2AX-marked DNA damages associated with
244 prolonged mitosis in mother cells activate p53 pathway in daughter cells that are non-diploid due to
245 chromosome missegregation, p53 upregulates the expression of its downstream target Rnd3 which
246 locally inhibits RhoA signaling and actomyosin contraction at cell-cell junctions, leading to
247 asymmetric RhoA activation at the rear cortex of daughter cells to drive cell internalization and
248 subsequent non-apoptotic death. Thus, this work uncovered a novel non-apoptotic mechanism by
249 mitosis for p53 to maintain genome integrity.

250 DNA damages associated with mitosis are generally phenotyped as prolonged mitosis or
251 mitotic arrest, which could also cause DNA damages (Dalton et al, 2007; Ganem & Pellman, 2012).
252 Formation of this vicious loop is largely due to impaired DNA damage response (DDR) which,
253 though being capable of sensing DNA damages, likely stops short of downstream damage repair
254 pathways (Heijink et al, 2013). Though activation of this partial DDR was believed to prevent fusion
255 of exposed telomeres under normal circumstance (Orthwein et al, 2014), it left unrepaired DNA
256 damages, pre-mitotic or acquired, into mitotic progenies under stressed conditions (Denchi & Li,
257 2014). Moreover, activation of the partial DDR during mitosis, instead helps fix errors in DNA,
258 actually could result in severe chromosome missegregation, which eventually gives rise to aneuploid
259 progenies (Bakhoum et al, 2017; Bakhoum et al, 2014). Therefore, surveillance mechanisms are
260 critical to deal with daughter cells from prolonged mitosis. Previous studies indicated that prolonged
261 mitotic progenies might be surveilled by either growth arrest or apoptosis (Joerger & Fersht, 2016;
262 Lambrus & Holland, 2017; Vitale et al, 2011). Whereas in this study, we identified a novel
263 surveillance mechanism executed by CIC-mediated non-apoptotic death termed mitosis. Although
264 also being activated by prolonged mitosis via p53-dependent pathway, mitosis likely represents a
265 unique process independent from growth arrest and apoptosis because depleting p21, a p53 downstream
266 effector that is required for growth arrest/senescence, didn't block mitotic CIC formation at all (data
267 not shown), and depletion of Rnd3, a p53 target gene that was identified as suppressor of ROCK I-

268 mediated apoptosis (Ongusaha et al, 2006; Paysan et al, 2016), significantly suppress mitosis
269 (Figure 5I-L).

270 Interestingly, while our work demonstrates a positive role of CIC formation in maintaining
271 genome stability by eliminating aneuploidy cells, previous work supported entosis as a cellular
272 mechanism to promote genome instability by inducing aneuploidy (Krajcovic et al, 2011). This clear
273 conceptual discrepancy is actually due to different cellular and molecular contexts where CIC
274 formation may work. At cellular level, Krajcovic *et al* found that the presence of inner cell could
275 physically block cytokinesis of outer cell, leading to outer cell binucleation and subsequent
276 aneuploidy of its offspring following next round of cell division (Krajcovic et al, 2011). This effect
277 may be propagated to promote genome instability in the context of tumor cells that are tolerated to
278 aneuploidy. This idea was supported by recent work in lung cancer cells Mackay *et al* (Mackay et
279 al, 2018). Whereas this work investigates CIC's role in a non-tumor context, in which aneuploid
280 daughters from prolonged mitosis were internalized as inner cells and eliminated. Thus, it's likely
281 that CIC formation affects genome stability differentially via inner cell and outer cell, respectively,
282 depending on cells' tolerance to aneuploidy. For tumor cells who are generally aneuploidy-tolerant,
283 CIC formation may promote genome instability by inducing cytokinesis failure of outer cells; for
284 non-transformed epithelial cells, CIC formation may function to counteract genome instability by
285 internalizing and eliminating aneuploid cells. Of note, since aneuploidy is toxic and lethal to non-
286 transformed cells, the aneuploid progenies of binucleated outer cells wouldn't survive for long
287 period (data not shown). This is also true for tumor cells that are not tolerant to aneuploidy (Mackay
288 et al, 2018). Therefore, CIC formation is genome instability- or tumor-suppressive anyway when
289 cells are not tolerant to aneuploidy. At molecular level, CIC's effects on aneuploidy and genome
290 stability are controlled by p53 status. Mackay *et al* found that only mutant p53, but not wild type or
291 null p53, could promote genome instability via CIC formation by conferring cancer cells
292 winner/outer identity and allowing survival and population of their aneuploidy progenies (Mackay

293 et al, 2018). Whereas, our work demonstrated that wild type p53 endowed loser/inner identity to
294 cells during CIC formation by facilitating the establishment of polarized RhoA activities. Together,
295 we propose that CIC formation, depending on p53 status, may play dual roles in genome instability
296 and tumorigenesis as well. For cancer cells with mutant p53, CIC formation plays promotive role
297 by facilitating selection of cancer cells harboring mutant p53; for normal epithelial cells or cancer
298 cells that contain wild type p53, CIC formation play suppressive role by eliminating aneuploidy
299 cells expressing wild type p53 through mitosis. It'll be of interest to explore whether other
300 oncogenic mutations may also regulate CIC's functional outcomes.

301 Recently, two other works reported entosis induction in confined contexts in adherent
302 monolayer cultures (Durgan et al, 2017; Hamann et al, 2017). One of work demonstrated that
303 glucose starvation, an extreme biological condition, was capable of promoting CIC formation
304 mainly in the context of cancer cells like MCF7 in an AMP activated protein kinase (AMPK)-
305 dependent way (Hamann et al, 2017). Interestingly, although AMPK is a well-known energy sensor,
306 it was found in mitotic apparatus and involved in the regulation of mitotic progression and
307 completion (Banko et al, 2011; Li & Zhang, 2017). So we hypothesize that glucose induced
308 activation of AMPK may influence normal mitosis, which triggers mitosis and contributes to CIC
309 formation in adherent cells that is yet to be validated. Another work reported that depletion of
310 CDC42, a polarity protein, induced CIC formation in 16HBE cells (Durgan et al, 2017). Although
311 mitosis was found linked to CIC formation, the work failed to identify the essential role of mitotic
312 arrest and DNA damages in CIC formation, hence, couldn't tell why most mitosis failed to give rise
313 to CIC structures and why reagents blocking mitosis unexpectedly induced CIC formation, therefore
314 no physiological roles were proposed. Intriguingly, similar to work by Wan et al (Wan et al, 2012),
315 where depletion of polarity protein PAR3 resulted in enhanced formation of CIC structures in
316 adherent MDCK cells, polarity changes were not regarded as the reason for enhanced CIC formation
317 (Durgan et al, 2017; Wan et al, 2012). Whereas, we found that depleting polarity protein such as

318 CDC42 in MCF10A and tumor cells could promote CIC formation that was also preceded by
319 prolonged mitosis (data not shown), we therefore speculate that altered mitosis might be a shared
320 route for multiple factors, such as glucose starvation and depleting polarity proteins and the like, to
321 activate mitosis that works in multiple contexts to maintain homeostasis.

322

323 **Materials and Methods:**

324 **Cell culture and constructs.** MCF7, PLC/PRF/5 and 293FT cells were maintained in Dulbecco's
325 modified Eagle's medium (DMEM) supplemented with 10% fetal bovine serum (PAN-Biotech).
326 MCF10A and its derivatives were cultured in DMEM/F12 supplemented with 5% horse serum
327 (GIBCO, #16050-122), 20 ng/ml EGF (Peprotech, #96-AF-100-15-100), 10 µg/ml insulin (Sigma,
328 I-5500), 0.5 µg/ml hydrocortisone (Macgene, CC103), and 100 ng/ml cholera toxin (Sigma, C8052).
329 pBabe-H2B-mCherry was a gift from Dr. Michael Overholtzer. pBabe-RhoA biosensor was a gift
330 of Dr. Klaus Hahn from Addgene (12602). pLKO-shp53 was a gift of Dr. Bob Weinberg from
331 Addgene (19119). GFP-p53 was a gift of Dr. Tyler Jacks from Addgene (12091). Expression
332 plasmid for GFP-Rnd3 was constructed by inserting synthesized human Rnd3 ORF into pQCXIP-
333 GFP vector by *Xho* I and *Bam*H I sties. Expression plasmid for MLC-mCherry was constructed by
334 inserting synthesized chicken MLC ORF into pBabe-mCherry vector by *Xho* I and *Bam*H I sties.

335 **Antibodies and chemical reagents.** Antibodies with working dilution factors, company source and
336 catalog number include: anti-pMLC (1:200; Cell Signaling; #3671), anti-E-cadherin (1:200; BD
337 Biosciences; 610181), anti-LAMP1 (1:200; Abcam; ab62562), anti-CD68 (1:200; Santa Cruz; sc-
338 20060), anti-c-Caspase3 (1:1500; Cell Signaling; #9664), anti-pH3 (1:100; Cell Signaling; #9764),
339 anti-β-catenin (1:200; Sigma; c2206), anti-MAD2 (1:200; Proteintech; 10337-1-AP), anti-HA
340 (1:1500; Cell Signaling; #3724), anti-γH2AX (1:200; Cell Signaling; #9718 for IF; 1:500; ABclonal;
341 AP0099 for WB), anti-H2AX (1:1000; ABclonal; AP0823), anti-pATM (1:500; Boster; BM4008),
342 anti-ATM (1:1000; Proteintech; 27156-1-AP), anti-pp53 (1:500; Cell Signaling; #9386), anti-p53
343 (1:1000; Santa Cruz; sc-126), anti-Rnd3 (1:1000; Sino Biological; 101056-T32). Secondary
344 antibodies include Alexa Fluor 568 anti-mouse (1:500; Invitrogen; A11031), Alexa Fluor 568 anti-
345 rabbit (1:500; Invitrogen; A11036), Alexa Fluor 488 anti-mouse (1:500; Invitrogen; A11029) and
346 Alexa Fluor 488 anti-rabbit (1:500; Invitrogen; A11034). Alexa Fluor®647 Phalloidin (1:200;
347 Invitrogen; A22287). DAPI was purchased from Sigma (D8417). ROCK inhibitor Y27632 was

348 purchased from TOCRIS (1254) and used at final concentration of 10 μ M. Colchicine (HY-16569),
349 Ro-3306 (HY-12529), a potent and selective inhibitor of CDK1, and SU-9516 (HY-18629), a
350 selective CDK2 inhibitor, were purchased from MedChem Express. DNA damage inducers
351 Mitomycin (T6890) and Bleomycin (T6116), and inhibitors for ATM (T2474), ATR (T3338),
352 CHK1 (T2033), CHK2 (T7080) were purchased from TargetMol. Collagen Type I is a product of
353 BD Biosciences (#354236).

354 **Virus production and infection.** Stable expression cell lines were established by virus infection.
355 Briefly, 1×10^6 293FT cells were plated into 6-well plate coated with collagen I (BD Bioscience,
356 #354236), transfection was performed with retroviral constructs together with packaging plasmids,
357 and viruses were collected twice at 24 h intervals. To infect cells, cells were cultured in 1 ml viral
358 supernatant mixed with 1 μ l polybrene of 10 μ g/ml stock for 6 h followed with regular media. Cells
359 were selected with appropriate antibiotics (2 μ g/ml puromycin or 400 μ g/ml G418 for MCF10A,
360 1 μ g/ml puromycin for MCF7 and PLC/PRF/5) for 7 days.

361 **RNA interference.** siRNAs were from GenPharma (Shanghai, China). For individual siRNA trans
362 fection, cells (1×10^5 /well) were plated into 12-well glass bottom plate and cultured overnight, then
363 transfected with 50 nM siRNA using Lipofectamine® RNAiMAX (Invitrogen, #13778-150). Cell
364 s were fed with fresh full media 6 h later. siRNA sequences: CUEDC2: 5'-CAUCAGAGGAGAA
365 CUUCGA-3'; CDC20: 5'-CCACCAUGAUGUUCGGGUATT-3'; MAD2 : 5'-GGAAGAGUCGG
366 GACCACAGTT-3'; BuBR1: 5'-CGGGCAUUUGAAUAUGAAATT-3'; ESPL1: 5'-GCUUGUGA
367 UGCCAUCCUGATT-3'; H2AX-1: 5'- GGGACGAAGCACUUGGUAACA-3'; H2AX-2: 5'- GAC
368 AACAGAAGACGCGAAUC-3'; p53-1: 5'- AAGACUCCAGUGGUAUAUCUAC-3'; p53-2: 5'- G
369 ACUCCAGUGGUAUAUCUAC-3'; Rnd3-1: 5'- GAUCCUAAUCAGAACGUGAAA-3'; Rnd3-2: 5
370 '- AUCCUAAUCAGAACGUGAAA-3'; ATM: 5'- GCCUCCAAUUCUUCACAGUAA-3'; ATR:
371 5'- GAUGAACACAUGGGGAUAUUUA-3'; CHK1-1: 5'- GUGACAGCUGUCAGGAGUAUU-3';
372 CHK1-2: 5'- GCCCACAUGUCCUGAUCAUAU-3'; CHK2-1: 5'- GAACAGAUAAAUACCGA

373 ACAU-3'; CHK2-2: 5'- CGCCGUCCUUUGAAUAACAAU-3'; Negative Control: 5'-UCUCCGA
374 ACGUGUCACGUTT-3'.

375 **Reverse transcription-quantitative PCR (RT-qPCR).** Total RNA was isolated from cells 48 h a
376 fter siRNA transfection using TRIzol reagent (Invitrogen, #15596026). One microgram of total RN
377 A was converted into cDNA using *TransScript*[®] One-Step gDNA Removal and cDNA Synthesis S
378 uperMix (Transgen Biotech, #AT311-02) according to manufacturer's instruction. The quantitativ
379 e PCR (qPCR) was performed on 15 ng of cDNA from each sample using SYBR Green Real-time
380 PCR Master Mix (TOYOBO, #QPK-201) based on the recommendations of manufacturer. Primers
381 pairs spanning at least two exons were confirmed by NCBI Primer-BLAST: CUEDC2: 5'-TGAG
382 CGATGCCAGGAACAA-3' and 5'-CTCCTCCTCAGCGCCAGTT-3'; CDC20: 5'-TTCCCTGCC
383 AGACCGTATCC-3' and 5'-CAGCCAAGTAGTTGCCCTC-3'; MAD2: 5'-TTCTCATTCGGCAT
384 CAACA-3' and 5'-TCTTTCCAGGACCTACCA-3'; BuBR1: 5'-TCTTCAGCAGCAGAAACGG
385 -3' and 5'-TCATTGCATAAACGCCCTA-3'; ESPL1: 5'-CCCCACTTCGGGCATTGTA-3' and 5'-
386 GGGCAAAGTCATAAACCACC-3'; CCNB1: 5'-AATAAGGCGAAGATCAACATGGC-3' and
387 5'-TTTGTTACCAATGTCCCCAAGAG-3'; BUB1: 5'-AGAAATACCACAATGACCCAA-3' and
388 5'-AGGCGTGTCTGAAATAACC-3'; AURKA: 5'-GCCCTGTCTTACTGTCATTCG-3' and 5'-A
389 GGTCTCTTGGTATGTGTTTGC-3'; CENPE: 5'-CCTTAACTTGTGGAGGTGGC-3' and 5'-AG
390 CGAACTGGATGAGGTGAT-3'; CENPA: 5'-GGCGGAGACAAGGTTGGCTAAA-3' and 5'-GG
391 CTTGCCAATTGAAGTCCACAC-3'; H2AX: 5'- CCCTTCCAGCAAACCTCAACTCG-3' and 5'-
392 AAACTCCCCAATGCCTAAGGT-3'; p53: 5'- ACCACCATCCACTACAACACTACAT-3' and 5'-
393 CTCCCAGGACAGGCACAAA-3'; Rnd3: 5'- TCTTACCCTGATTCGGATGC-3' and 5'- TCTGA
394 CGTATTTTCCGACT-3'; ATM: 5'- GCACAGAAGTGCCTCCAATTC-3' and 5'- ACATTCTG
395 GCACGCTTTG-3'; ATR: 5'- GCCGTTCTCCAGGAATACAG-3' and 5'- GAGCAACCGAGCTT
396 GAGAGT-3'; CHK1: 5'- GGATGCGGACAAATCTTACCA-3' and 5'- CCTTAGAAAGTCGGA
397 AGTCAACC-3'; CHK2: 5'- GTCATCTCAAGAAGAGGACT-3' and 5'- GAGCTGTGGATTCAT

398 TTTCC-3'; HPRT: 5'-AGGCCATCACATTGTAGCCCTCTGT-3' and 5'-TACTGCCTGACCAA
399 GGAAAGCAAAGT-3'. The PCR reactions run on the following conditions: initial denaturing at 9
400 5°C for 30 sec, followed by 35–40 cycles of 95°C for 5 sec, 60°C for 10 sec and 72°C for 15 sec,
401 melting curves were examined at 37°C for 30 sec before cooling. Each result was from three indep
402 endent biological replicates for all analyses performed in this work. The qPCR results were analyz
403 ed using $2^{-\Delta\Delta C_T}$ method and presented as relative quantity of transcripts with HPRT as the referenc
404 e gene.

405 **Cytospin and entotic CIC quantification.** Described protocol (Sun & Overholtzer, 2013) was
406 slightly modified to examine cells abilities to form CIC structures. Briefly, cells were cultured in
407 suspension for 6 h in 6-well plate pre-coated with 1 ml solidified soft agar (0.5%) and then mounted
408 onto glass slides for 3-min centrifugation at 400 rpm to make cytopsin. Cells were fixed by 4% PFA
409 and immunostained with E-cadherin antibodies followed by mounting with Antifade reagent with
410 DAPI. CIC structures with more than half of cell body internalized were counted.

411 **Time lapse imaging and mitotic CIC quantification.** Wide field imaging was performed on cells
412 plated in glass bottom dish or plate (Nest Biotechnology Co.) by Nikon Ti-E microscope equipped
413 with motorized stage and Neo Vacuum cooled Scientific CMOS Camera (Andor Technology).
414 Images were collected every 10 or 15 min for 24 h using 10x or 20x Apo objective lens with 15 ms
415 exposure for DIC channel and 150 ms exposure for mCherry channel. Cells were cultured in
416 humidified chamber supplied with 5% CO₂ at 37°C during imaging. Image sequences were reviewed
417 using Nikon NIS-Elements AR 4.5 software. Mitotic entry was judged morphologically by either
418 condensed chromatin as indicated by H2B-mCherry condensation or cells' round up. Mitotic
419 anaphase was judged by chromosome separation labeled with H2B-mCherry. The duration of
420 metaphase was determined from the first frame of mitotic entry to the first frame of mitotic anaphase.
421 CIC structures were determined morphologically by complete enwrapping of cells into their
422 neighbors, typically with a crescent nucleus in the outer cells. Total cells in each field were counted

423 on mCherry-positive nuclei. CIC frequency was presented as CIC number divided by total cells in
424 each field.

425 For CIC formation induced by DNA damages, MCF10A/H2B-mCherry cells in 12 well plate
426 (2.5×10^4 /well) were synchronized by 100ng/ml nocodazole for 6 h followed by treatment of DNA
427 damage inducers mitomycin (0.5 μ M, 1 μ M, 2 μ M) for 3.5 h. Then, drugs were washed out for 20
428 h time lapse in full medium. CIC formation was quantified as did above.

429 **Time lapse-associated FISH (fluorescence in situ hybridization).** Prior to FISH, MCF10A cells
430 of 3×10^5 were first cultured in gridded glass bottom dish (μ -Dish 35mm Grid-500, ibidi; #81168)
431 for 20 h, followed by time lapse microscopy with images collected every 10 min for 16 h by using
432 10x Apo objective lens in DIC channel. Then, cells were immediately fixed at room temperature for
433 20 min with freshly prepared solution (methanol/glacial acetic acid = 3:1) after briefly washed twice
434 with PBS. Fixed cells were initially baked at 56 °C for 60 min, subsequently incubated in 100 μ g/ml
435 RNase (pH=7.0 \pm 0.2) for 1 h and then 20 mg/ml pepsin-0.01 M HCl for 10 min at 37 °C. After
436 washed twice with 2 \times SSC at room temperature for 5 min, samples were dehydrated in 70%, 85%,
437 and 100% pre-cooled ethanol for 2 min respectively, and then air-dried. Hybridization was
438 performed with two-probe FISH kit (F01010-00, GP Medical Technologies, Ltd) following the
439 manual provided. Briefly, sample was denatured at 75°C for 10 min and then preceded to
440 hybridization at 42°C for 16 h in a humidified cassette. Following hybridization, sample was serially
441 washed with 0.4x SSC containing 0.3% NP-40 (pH=7.0 \pm 0.2) at 65 °C for 3 min, 2x SSC containing
442 0.1% NP-40 (pH=7.0 \pm 0.2) at room temperature for 1 min and finally 70% ethanol at room
443 temperature for 3 min before counterstained with DAPI in darkness for 10-15 min and mounted.
444 Images were taken by using *Ultraview Vox* spinning disc confocal system (Perkin Elmer) equipped
445 with a Yokogawa CSU-X1 spinning disc head and EMCCD camera (Hamamatsu C9100-13) on
446 Nikon Ti-E microscope. Analysis was performed with Volocity software (Perkin Elmer).

447 Information on cell position, division and CIC formation were determined based on time lapse
448 imaging and grids on the glass bottom.

449 **Time lapse-associated immunostaining (TLAS).** For phospho-Myosin Light Chain 2 (pMLC)
450 staining in mitotic cells, MCF10A/H2B-mcherry cells in gridded glass bottom dish (μ -Dish 35mm
451 Grid-500) were transfected with CDC20 siRNA as described above. Time lapse imaging was
452 performed by 10x Apo objective lens in DIC and mCherry channels next day, with images captured
453 every 10 min for 4 h before fixing with 4% PFA and preceded to routine staining. Briefly, the fixed
454 sample was permeabilized with 0.2% Triton-X 100/PBS for 5 min and blocked with 5% BSA for 1
455 h before incubated with primary antibody at 4°C overnight followed fluorophore-labeled secondary
456 antibody, cells were then co-stained with phalloidin and DAPI for 20 min and then mounted with
457 Prolong Gold antifade reagent (Invitrogen). Images were captured with Nikon Ti-E microscope
458 equipped with Neo Vacuum cooled Scientific CMOS Camera (Andor Technology) and analyzed
459 with Nikon NIS-Elements AR 4.5 software. Mean pMLC intensity of individual cell was calculated
460 by equation: (pMLC-background)/area. TLAS of γ H2AX and p53 were performed following the
461 protocol for pMLC with slight modification that time lapse was performed for 20 h in control or
462 CUEDC2-depleted MCF10A cells.

463 **Immunostaining and Immunoblotting.** Cultured cells were stained following protocol above in
464 TLAS. For tissue sections, samples were first deparaffinized and antigen retrieved following routine
465 procedures and then preceded to immunostaining as did in fixed cells above. Confocal images were
466 captured and processed by *Ultraview Vox* confocal system (Perkin Elmer) on Nikon Ti-E
467 microscope. Immunoblotting was performed following standard precedures, briefly, protein
468 samples were separated by SDS-PAGE and then transferred onto PVDF membrane, where specific
469 antibodies were used to probe target proteins.

470 **FRET.** Briefly, activation levels of RhoA were measured by monitoring the ratio of ECFP to
471 Citrine-YFP FRET and ECFP intensities (Pertz et al, 2006; Sun et al, 2014a). Images were acquired

472 on a Nikon Ti-E inverted microscope using a Neo Vacuum cooled Scientific CMOS Camera (Andor
473 Technology) mounted on the bottom port with a set of excitation/emission filter wheels to direct the
474 DIC, ECFP, FRET, and Citrine-YFP signals sequentially. Images were obtained using a Nikon
475 20x/0.75 CFI Plan Apochromat Lambda lens and Nikon NIS-Elements AR 4.5 software. The filter
476 sets used for ratiometric imaging were (Excitation, emission, respectively, Chroma Technology):
477 ECFP: ET438/24, ET482/35; FRET: ET438/24, ET540/30; and Citrine-YFP: ET513/17, ET540/30.
478 Cells were illuminated by LUMENCOR SPECTRA X Light Engine with 438/24 and 513/17
479 excitation filters. CFP, FRET and DIC images were recorded with 1 x 1 binning. The FRET module
480 of Nikon NIS-Elements AR 4.5 software was used to process image sequences. The background-
481 subtracted images from two cameras were aligned to ascertain optimal registration with subpixel
482 accuracy. A linear rainbow pseudocolor lookup table was applied to the ratiometric images.

483 **Patient samples.** Breast cancer sections were obtained from 307 Hospital under the hospital's
484 regulations and ethics. Sections stained with E-cadherin or HER2 were scanned by NanoZoomer-
485 SQ (Hamamatsu) digital slide scanning system. CIC structures were judged by fully enclosing of
486 one or more cells within another cell based on membrane contour line. Patient sections were first
487 screened based on the number of CIC structures in fields of 40x magnification, those that had less
488 than 1 CIC structures in more than 3 fields were scored as low CIC, more than 15 CIC structures in
489 3 fields as high CIC, the rest as medium CIC.

490 **Statistics.** All assays were carried out in triplicate or more. Data were expressed as means with
491 standard deviations (SD) or standard error of mean (SEM). *P*-values were calculated using two-
492 tailed Student's t-test from Excel or GraphPad Prism software, and *P*-values less than 0.05 were
493 considered statistically significant. Logistic regression analysis in Excel was used to evaluate
494 association between factors.

495

496 **H2: Supplementary Materials**

497 Figure S1. Working model for p53-dependent postmitotic surveillance by mintosis.

498 Figure S2. Entosis is coupled with mitotic cell division.

499 Figure S3. Prolonged mitosis primes cells to undergo entosis.

500 Figure S4. Involvement of DNA damage-p53 pathway in mintosis.

501 Figure S5. Compartmentalized RhoA activity by Rnd3 is required for mintosis.

502 Figure S6. Mintosis selectively targets non-diploid cells for elimination.

503 Movie S1. The formation of entotic CIC structures.

504 Movie S2. Entosis is coupled with mitotic cell division.

505 Movie S3. Inner cell fates in CIC structures.

506 Movie S4. Catastrophic cell death of mitosis.

507 Movie S5. Mitosis of different metaphase.

508 Movie S6. RhoA activity by FRET during one-cell mintosis.

509 Movie S7. Time lapse for FISH.

510

511

512 **References and Notes**

- 513 Bakhoum SF, Kabeche L, Compton DA, Powell SN, Bastians H (2017) Mitotic DNA Damage Response: At the
514 Crossroads of Structural and Numerical Cancer Chromosome Instabilities. *Trends in cancer* **3**: 225-234
515
- 516 Bakhoum SF, Kabeche L, Murnane JP, Zaki BI, Compton DA (2014) DNA-damage response during mitosis induces
517 whole-chromosome missegregation. *Cancer discovery* **4**: 1281-1289
518
- 519 Banko MR, Allen JJ, Schaffer BE, Wilker EW, Tsou P, White JL, Villen J, Wang B, Kim SR, Sakamoto K, Gygi SP,
520 Cantley LC, Yaffe MB, Shokat KM, Brunet A (2011) Chemical genetic screen for AMPK α 2 substrates uncovers a
521 network of proteins involved in mitosis. *Molecular cell* **44**: 878-892
522
- 523 Bieging KT, Mello SS, Attardi LD (2014) Unravelling mechanisms of p53-mediated tumour suppression. *Nature*
524 *reviews Cancer* **14**: 359-370
525
- 526 Dalton WB, Nandan MO, Moore RT, Yang VW (2007) Human Cancer Cells Commonly Acquire DNA Damage
527 during Mitotic Arrest. *Cancer research* **67**: 11487-11492
528
- 529 Denchi EL, Li J (2014) Let it go: how to deal with a breakup in mitosis. *Nature structural & molecular biology* **21**:
530 433-435
531
- 532 Durgan J, Tseng YY, Hamann JC, Domart MC, Collinson L, Hall A, Overholtzer M, Florey O (2017) Mitosis can
533 drive cell cannibalism through entosis. *eLife* **6**: 1-26
534
- 535 Florey O, Kim SE, Sandoval CP, Haynes CM, Overholtzer M (2011) Autophagy machinery mediates macroendocytic
536 processing and entotic cell death by targeting single membranes. *Nat Cell Biol* **13**: 1335-1343
537
- 538 Funk LC, Zasadil LM, Weaver BA (2016) Living in CIN: Mitotic Infidelity and Its Consequences for Tumor
539 Promotion and Suppression. *Developmental cell* **39**: 638-652
540
- 541 Gadea G, de Toledo M, Anguille C, Roux P (2007) Loss of p53 promotes RhoA-ROCK-dependent cell migration and
542 invasion in 3D matrices. *The Journal of cell biology* **178**: 23-30
543
- 544 Ganem NJ, Pellman D (2012) Linking abnormal mitosis to the acquisition of DNA damage. *The Journal of cell*
545 *biology* **199**: 871-881
546
- 547 Gao YF, Li T, Chang Y, Wang YB, Zhang WN, Li WH, He K, Mu R, Zhen C, Man JH, Pan X, Li T, Chen L, Yu M,
548 Liang B, Chen Y, Xia Q, Zhou T, Gong WL, Li AL, Li HY, Zhang XM (2011) Cdk1-phosphorylated CUEDC2
549 promotes spindle checkpoint inactivation and chromosomal instability. *Nature cell biology* **13**: 924-933
550
- 551 Hamann JC, Surcel A, Chen R, Teragawa C, Albeck JG, Robinson DN, Overholtzer M (2017) Entosis Is Induced by
552 Glucose Starvation. *Cell Rep* **20**: 201-210
553
- 554 Heijink AM, Krajewska M, van Vugt MA (2013) The DNA damage response during mitosis. *Mutation research* **750**:
555 45-55
556
- 557 Joerger AC, Fersht AR (2016) The p53 Pathway: Origins, Inactivation in Cancer, and Emerging Therapeutic
558 Approaches. *Annual review of biochemistry* **85**: 375-404
559
- 560 Kapanidou M, Curtis NL, Bolanos-Garcia VM (2017) Cdc20: At the Crossroads between Chromosome Segregation
561 and Mitotic Exit. *Trends Biochem Sci* **42**: 193-205
562
- 563 Krajcovic M, Johnson NB, Sun Q, Normand G, Hoover N, Yao E, Richardson AL, King RW, Cibas ES, Schnitt SJ,
564 Brugge JS, Overholtzer M (2011) A non-genetic route to aneuploidy in human cancers. *Nat Cell Biol* **13**: 324-330
565
- 566 Kroemer G, Perfettini J-L (2014) Entosis, a key player in cancer cell competition. *Cell Res* **24**: 1280-1281
567
- 568 Kruiswijk F, Labuschagne CF, Vousden KH (2015) p53 in survival, death and metabolic health: a lifeguard with a
569 licence to kill. *Nature reviews Molecular cell biology* **16**: 393-405
570

- 571 Lambrus BG, Holland AJ (2017) A New Mode of Mitotic Surveillance. *Trends in cell biology* **27**: 314-321
572
- 573 Li Z, Zhang X (2017) Kinases Involved in Both Autophagy and Mitosis. *International journal of molecular sciences*
574 **18**
575
- 576 Liang J, Fan J, Wang M, Niu Z, Zhang Z, Yuan L, Tai Y, Chen Z, Song S, Wang X, Liu X, Huang H, Sun Q (2018)
577 CDKN2A inhibits formation of homotypic cell-in-cell structures. *Oncogenesis* **7**: 1-8
578
- 579 Mackay HL, Moore D, Hall C, Birkbak NJ, Jamal-Hanjani M, Karim SA, Phatak VM, Pinon L, Morton JP, Swanton
580 C, Le Quesne J, Muller PAJ (2018) Genomic instability in mutant p53 cancer cells upon entotic engulfment. *Nat*
581 *Commun* **9**: 3070
582
- 583 Musacchio A (2015) The Molecular Biology of Spindle Assembly Checkpoint Signaling Dynamics. *Current biology* :
584 *CB* **25**: R1002-1018
585
- 586 Ning X, Luo T, Chen Z, Sun Q (2015) The physics for the formation of cell-in-cell structures. *Current molecular*
587 *medicine* **15**: 867-872
588
- 589 Ongusaha PP, Kim HG, Boswell SA, Ridley AJ, Der CJ, Dotto GP, Kim YB, Aaronson SA, Lee SW (2006) RhoE is a
590 pro-survival p53 target gene that inhibits ROCK I-mediated apoptosis in response to genotoxic stress. *Current*
591 *biology* : *CB* **16**: 2466-2472
592
- 593 Orthwein A, Fradet-Turcotte A, Noordermeer SM, Canny MD, Brun CM, Strecker J, Escribano-Diaz C, Durocher D
594 (2014) Mitosis inhibits DNA double-strand break repair to guard against telomere fusions. *Science* **344**: 189-193
595
- 596 Overholtzer M, Mailleux AA, Mouneimne G, Normand G, Schnitt SJ, King RW, Cibas ES, Brugge JS (2007) A
597 nonapoptotic cell death process, entosis, that occurs by cell-in-cell invasion. *Cell* **131**: 966-979
598
- 599 Paysan L, Piquet L, Saltel F, Moreau V (2016) Rnd3 in Cancer: A Review of the Evidence for Tumor Promoter or
600 Suppressor. *Molecular cancer research* : *MCR* **14**: 1033-1044
601
- 602 Pertz O, Hodgson L, Klemke RL, Hahn KM (2006) Spatiotemporal dynamics of RhoA activity in migrating cells.
603 *Nature* **440**: 1069-1072
604
- 605 Ranjan A, Iwakuma T (2016) Non-Canonical Cell Death Induced by p53. *International journal of molecular sciences*
606 **17**
607
- 608 Riento K, Guasch RM, Garg R, Jin B, Ridley AJ (2003) RhoE binds to ROCK I and inhibits downstream signaling.
609 *Molecular and cellular biology* **23**: 4219-4229
610
- 611 Ruan B, Wang C, Chen A, Liang J, Niu Z, Zheng Y, Fan J, Gao L, Huang H, Wang X, Sun Q (2018a) Expression
612 profiling identified IL-8 as a regulator of homotypic cell-in-cell formation. *BMB Rep* **51**: 412-417
613
- 614 Ruan B, Zhang B, Chen A, Yuan L, Liang J, Wang M, Zhang Z, Fan J, Yu X, Zhang X, Niu Z, Zheng Y, Gu S, Liu X,
615 Du H, Wang J, Hu X, Gao L, Chen Z, Huang H, Wang X, Sun Q (2018b) Cholesterol inhibits entotic cell-in-cell
616 formation and actomyosin contraction. *Biochem Biophys Res Commun* **495**: 1440-1446
617
- 618 Santaguida S, Amon A (2015) Short- and long-term effects of chromosome mis-segregation and aneuploidy. *Nature*
619 *reviews Molecular cell biology* **16**: 473-485
620
- 621 Sivakumar S, Gorbisky GJ (2015) Spatiotemporal regulation of the anaphase-promoting complex in mitosis. *Nature*
622 *reviews Molecular cell biology* **16**: 82-94
623
- 624 Sun Q, Cibas ES, Huang H, Hodgson L, Overholtzer M (2014a) Induction of entosis by epithelial cadherin
625 expression. *Cell Res* **24**: 1288-1298
626
- 627 Sun Q, Luo T, Ren Y, Florey O, Shirasawa S, Sasazuki T, Robinson DN, Overholtzer M (2014b) Competition
628 between human cells by entosis. *Cell Res* **24**: 1299-1310
629
- 630 Sun Q, Overholtzer M (2013) Methods for the Study of Entosis. In *Methods in Mol Biol-Necrosis*, McCall K, Klein C
631 (eds), Vol. 1004, 5, pp 59-66. Humana Press

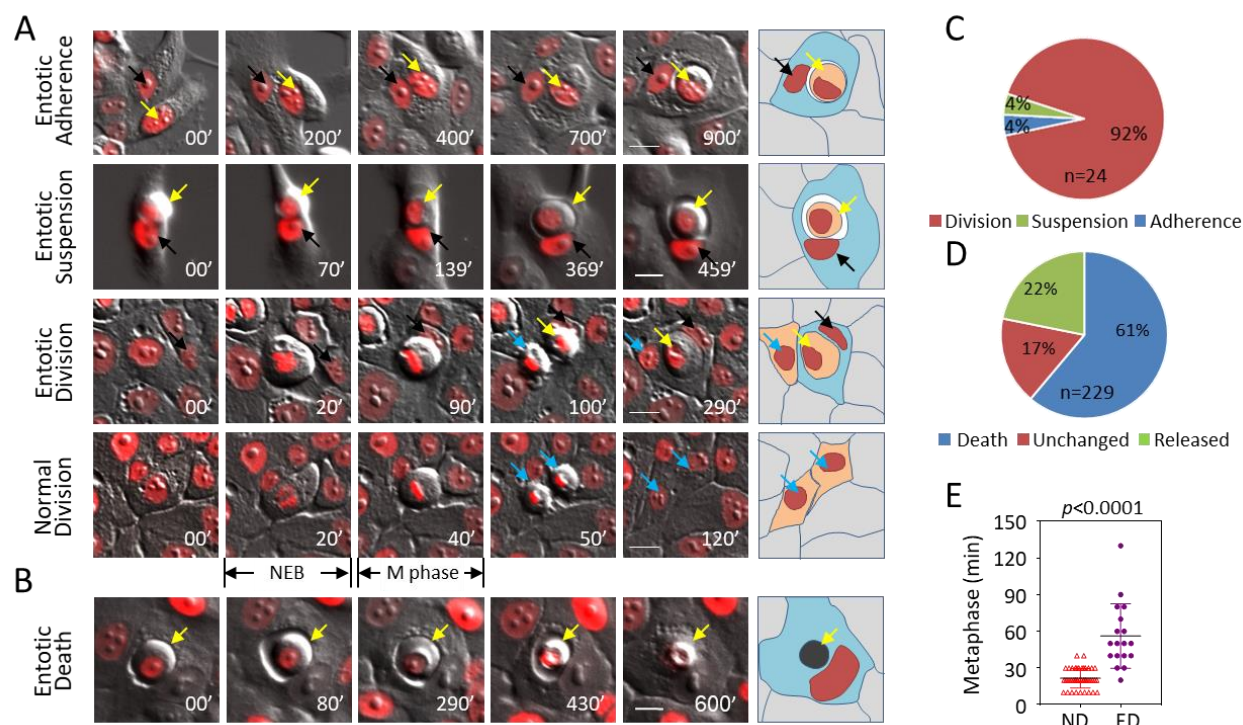
- 632
633 Vitale I, Galluzzi L, Castedo M, Kroemer G (2011) Mitotic catastrophe: a mechanism for avoiding genomic
634 instability. *Nature reviews Molecular cell biology* **12**: 385-392
635
636 Wan Q, Liu J, Zheng Z, Zhu H, Chu X, Dong Z, Huang S, Du Q (2012) Regulation of myosin activation during cell-
637 cell contact formation by Par3-Lgl antagonism: entosis without matrix detachment. *Mol Biol Cell* **23**: 2076-2091
638
639 Wennerberg K, Forget MA, Ellerbroek SM, Arthur WT, Burridge K, Settleman J, Der CJ, Hansen SH (2003) Rnd
640 proteins function as RhoA antagonists by activating p190 RhoGAP. *Current biology : CB* **13**: 1106-1115
641
642 Xia M, Land H (2007) Tumor suppressor p53 restricts Ras stimulation of RhoA and cancer cell motility. *Nature*
643 *structural & molecular biology* **14**: 215-223
644
645 Zhu Y, Zhou J, Xia H, Chen X, Qiu M, Huang J, Liu S, Tang Q, Lang N, Liu Z, Liu M, Zheng Y, Bi F (2014) The
646 Rho GTPase RhoE is a p53-regulated candidate tumor suppressor in cancer cells. *International journal of oncology*
647 **44**: 896-904
648
649

650 **Acknowledgments**

651 We thank Dr. Overholtzer from Memorial Sloan-Kettering Cancer Center for providing cell lines
652 and reagents. We thank Dr. Louis Hodgson from Albert Einstein College of Medicine of Yeshiva
653 University for assistance in FRET. We thank Dr. Dangsheng Li for discussions and critical reading
654 of the manuscript. **Funding:** This work was supported by the National Key Research &
655 Development Program of China (2016YFC1303303, 2018YFA0900804), the National Basic
656 Research Program of China (2015CB553704), the National Natural Science Foundation of China
657 (81572799, 31671432, 81872314, 81471578, 31770975). **Author contributions:** Q.S. conceived
658 the project and conception. Q.S., H.H. and J.L. designed experiments with the advice from X.N.W.
659 and Z.C.. J.L. performed majority of the experiments with the assistance of X.Y. for RNA
660 interference, phenotype and qPCR, and Z.N. for pathology, immunostaining and FISH. M.W. B.Z.
661 and H.Q helped in protein expression and detection. S.G. and L.G. assisted imaging. Y.T. provided
662 patient samples and related information. Q.S., H.H. and J.L. analyzed the data with the assistance
663 of Y.Z.. Q.S. and J.L. wrote the paper with input from X.N.W, L.M. and H.H., and all authors
664 reviewed the manuscript. **Competing interests:** no conflict of interest to be stated.

665

666 **Figures**



667
668

Figure 1. Entosis is preceded by mitosis of prolonged metaphase.

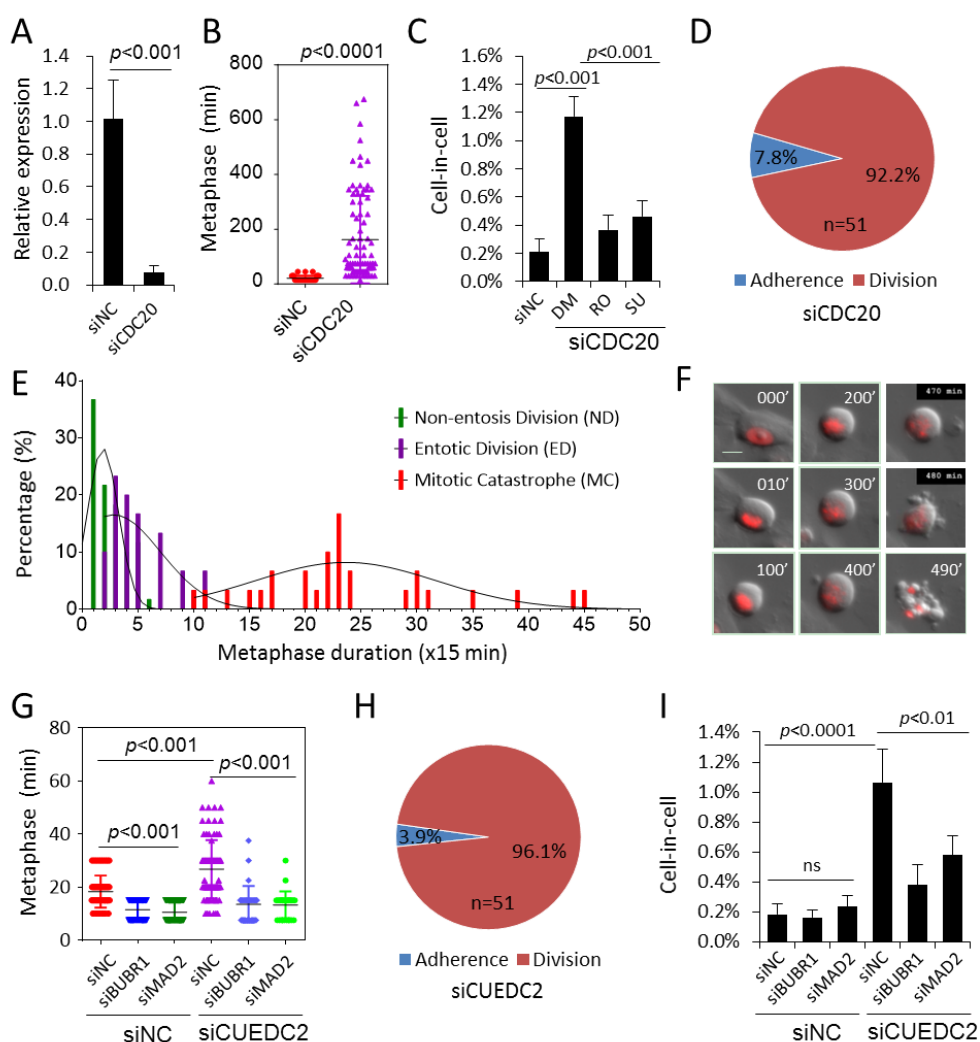
669 (A) Representative image sequences for the formation of entotic CIC structures from adherent cell (panel of
670 Entotic Adherence), suspended cells (panel of Entotic Suspension), divided cells (panel of Entotic
671 Division), and normal cell division (panel of Normal Division). Yellow arrows indicate internalized cells,
672 black arrows indicate outer cells, blue arrows indicate cells adhered to plate bottom. NEB: nuclear
673 envelop breakdown; Scale bar: 20 μ m. Also see Movie S1.

674 (B) Representative image sequences for inner cell death of entotic CIC structures in MCF10A cells. Arrows
675 indicate inner cell. Scale bar: 20 μ m.

676 (C) Quantification of Entotic Adherence (Adherence), Entotic suspension (Suspension) and Entotic Division
677 (Division). Quantification of inner cell fates in entotic CIC structures over 24 h period in MCF10A cells.
678 Also see Movie S3.

679 (D) Metaphase analysis of normal cell division (ND) and entotic cell division (ED) referring to cell division
680 leading to entotic CIC formation in MCF10A cells. n=52 for ND, 18 for ED.

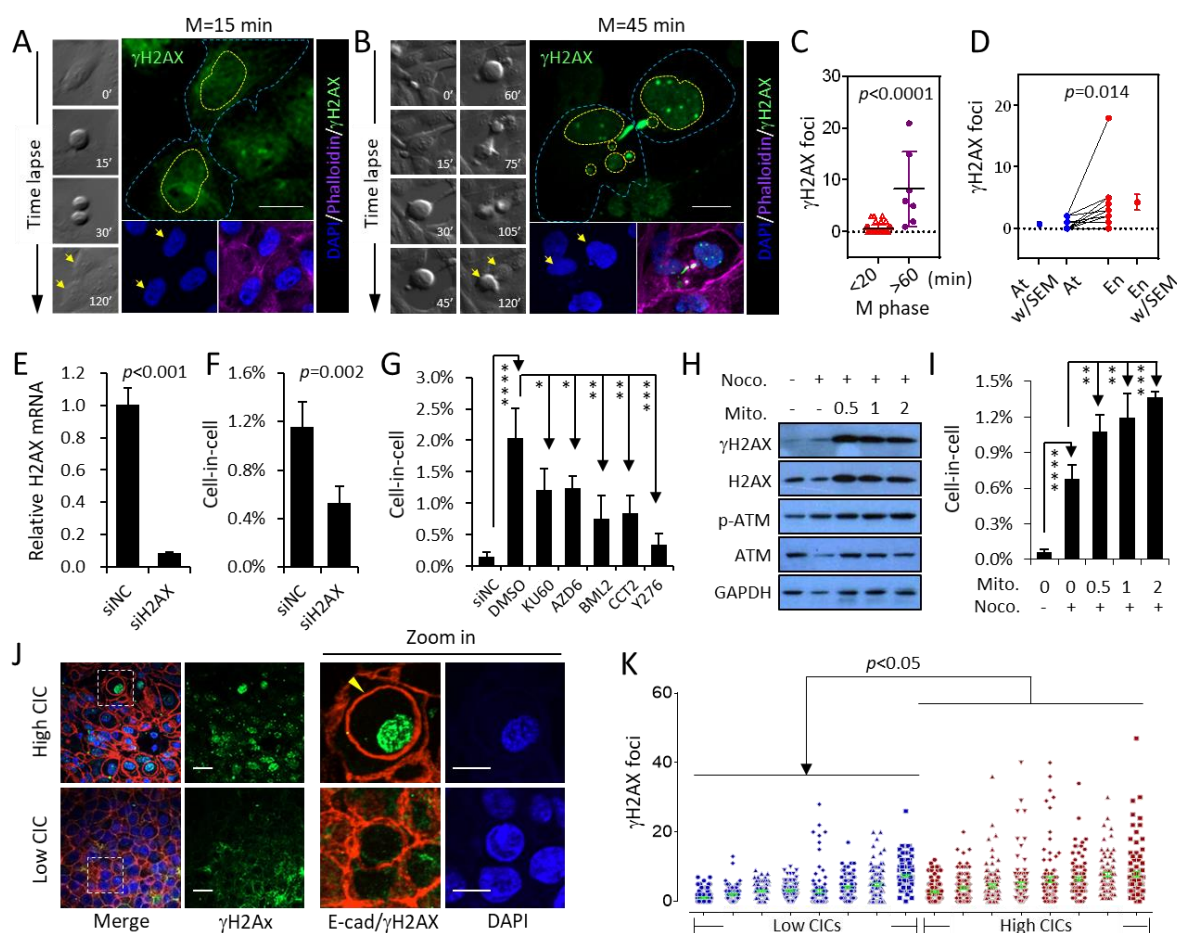
681



682
683

Fig. 2. Prolonged mitosis primes cells to undergo entosis.

- 684 (A) CDC20 mRNA level examined by quantitative PCR (qPCR) upon knockdown by RNA interference. Data are
685 mean \pm SD of triplicate experiments. $p < 0.001$.
- 686 (B) Graph plots metaphase duration of control (siNC, $n = 30$) and CDC20 depleted (siCDC20, $n = 90$) cells.
687 $p < 0.0001$.
- 688 (C) Quantification of CIC structures in control (siNC) and CDC20 (siCDC20) depleted cells. DM: DMSO; RO:
689 Ro-3306(10 μ M); SU: SU-9516 (5 μ M). Data are mean \pm SD of 4 or more fields with more than 5000 cells
690 analyzed each. $p < 0.001$ for the pairs of siNC vs DM, DM vs RO, DM vs SU.
- 691 (D) Quantification of Entotic Adherence (Adherence) and Entotic Division (Division) in MCF10A cells with
692 CDC20 depletion.
- 693 (E) Histogram analysis with fitted curves of metaphase from non-entosis division (ND), entotic division (ED) and
694 mitotic catastrophe (MC). $n = 30$ for ND and MC, 24 for ED. Gaussian curve was created by nonlinear
695 regression of the frequency distribution by GraphPad Prism software.
- 696 (F) Image sequence shows example of mitotic catastrophe with 490 min metaphase. Also see Movie S4. Scale
697 bar: 20 μ m
- 698 (G) Graph plots metaphase duration of control (siNC) and CUEDC2, BUBR1 and MAD2 depleted cells. From
699 left to right, $n = 58, 60, 60, 85, 30, 30$, respectively. $p < 0.001$ between pairs analyzed as indicated.
- 700 (H) Quantification of Entotic Adherence (Adherence) and Entotic Division (Division) in MCF10A cells with
701 CUEDC2 depletion.
- 702 (I) Quantification of CIC structures in cells co-depleting CUEDC2 with BUBR1 or MAD2 genes. Data are mean
703 \pm SD of 4 or more fields with more than 5000 cells analyzed each. ns: not significant. $p < 0.0001$ between
704 siCUEDC2 and siNCs, $p < 0.01$ between siNC and siBUBR1 or siMAD2 within siCUEDC2 group.
705

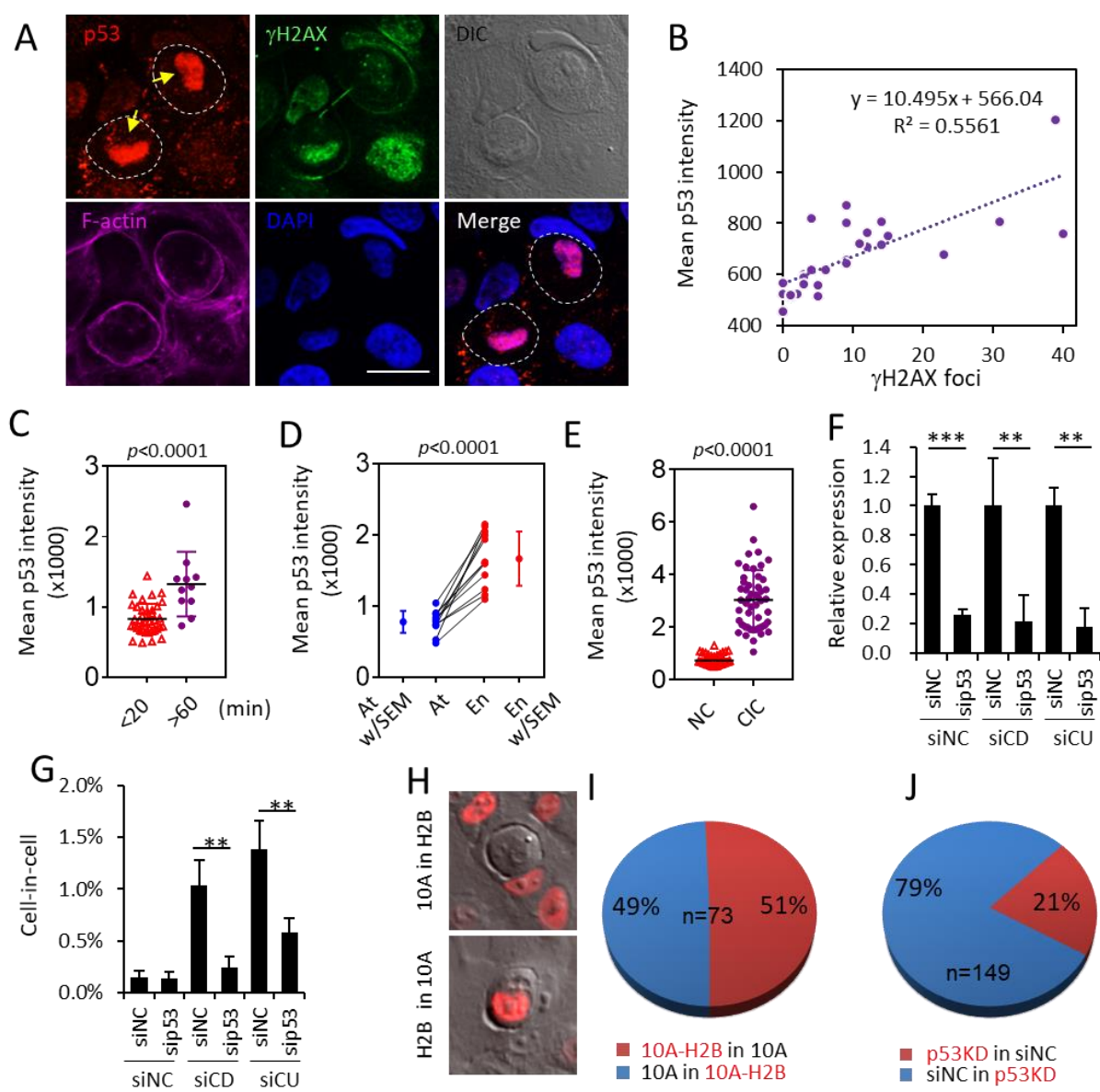


706
707

Figure 3. Mitotic DNA damages promote mitosis.

- 708 (A-B) Representative images for time lapse-associated immunostaining of γ H2AX in mitotic cells of short M
709 phase (A, 15 min) and long M phase (B, 45 min), with corresponding DIC images of time lapse on the left
710 and images for DAPI and merge channels on the bottom. Arrows indicate sibling cells. Blue dashed lines
711 depict cell shape, yellow dashed lines depict shape of nuclei. Note: sibling cells from long M phase (B, 45
712 min) contain micronuclei indicating chromosome missegregation, and multiple γ H2AX foci indicating DNA
713 damages. Scale bar: 10 μ m.
- 714 (C) Number of nuclear γ H2AX foci in cells from mitosis of different M phases. n=48 for M phase<20 min and 7
715 for M phase>60 min.
- 716 (D) Number of nuclear γ H2AX foci in paired sibling cells with one attached to the culture bottom (At) while
717 another internalized to form CIC structure (En). n=12.
- 718 (E-F) H2AX depletion (E) inhibits mitotic CIC formation (F). Data are mean \pm SD of 4 or more fields with more
719 than 5000 cells analyzed each.
- 720 (G) Effects of inhibiting DDR signaling on mitotic CIC formation in CUEDC2-depleted cells by compounds
721 targeting ATM (KU60 for KU-60019), ATR (AZD6 for AZD6738), CHK1 (BML2 for BML-277) and CHK2
722 (CCT2 for CCT245737). Inhibition of ROCKs by Y27632 (Y276) as positive control. Data are mean \pm SD
723 of 4 or more fields with more than 4000 cells analyzed each. siNC for non-target control siRNA.
- 724 (H) DNA damages by mitomycin (Mito.) increase expression of γ H2AX and phospho-ATM in cells synchronized
725 in M phase by nocodazole (Noco.).
- 726 (I) Formation of mitotic CIC structures in cells 18 hours released from mitotic arrest under conditions in (H).
727 Data are mean \pm SD of 4 or more fields with more than 4000 cells analyzed each.
- 728 (J) Representative images for γ H2AX staining in breast cancer tissues. E-cadherin (E-cad) in red indicates cell
729 junctions. Arrow head indicates inner cell of a CIC structure. Scale bars: 20 μ m for the left, 10 μ m for zoomed
730 images in the right.
- 731 (K) Quantification of nuclear γ H2AX foci in 16 human breast cancer samples. About one hundred of cells were
732 quantified for each sample.

733



734

735

Figure 4 p53 signaling pathway is required for mitosis.

736

(A) Representative images for p53 staining in daughter cells forming CIC structures as indicated by yellow arrows. Scale bar is 10 μ m.

737

(B) Correlation analysis between p53 expression and number of nuclear γ H2AX foci in MCF10A cells. n=30.

738

(C) Expression of p53 as indicated by mean staining intensity in cells from mitosis of different M phases. n=38 for M phase <20 min and 11 for M phase >60 min.

739

(D) Expression of p53 in paired sibling cells with one attached to the culture bottom (At) while another internalized to form CIC structure (En). n=12.

740

(E) Expression of p53 in inner cells of fresh CIC structures (CIC) is higher than that in single mono-nucleic cell (NC). n=50 for each group.

741

(F-G) p53 depletion (sip53) inhibits mitotic CIC formation induced by CDC20 (siCD) and CUEDC2 (siCU) knockdown. siNC for non-target control siRNA.

742

(H-J) Reduced frequency for p53 knockdown (p53KD) cells (labeled with H2B-mCherry in (J)) to penetrate into control cells (siNC). siNC for non-target control siRNA.

743

744

745

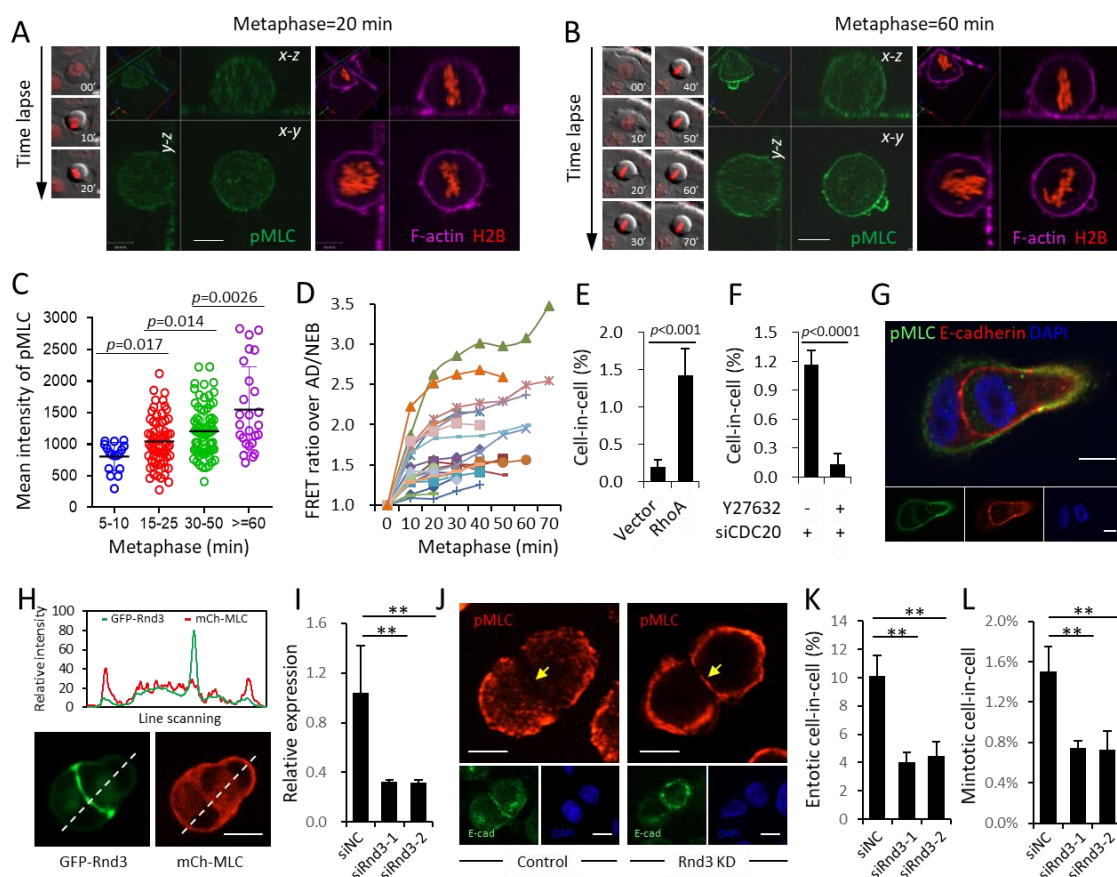
746

747

748

749

750



751
752 **Figure 5. Rnd3 is required for asymmetric RhoA activation and mitotic CIC formation.**

753 (A-B) Representative image of pMLC staining in mitotic cell of normal metaphase (20 min) (A) or prolonged
754 metaphase (60 min) (B), with corresponding DIC/mCherry images of time lapse on the left and F-actin
755 staining on the right. Scale bar: 10 μ m. Also see Movie S5.

756 (C) Graph plots pMLC mean intensity in mitotic cells of different metaphase duration as indicated. From left to
757 right, n=17, 67, 75, 26, respectively. Mean pMLC intensity of individual cell was calculated by normalization
758 of background-subtracted pMLC intensity over cell area. Data are mean \pm SD of 20 fields with totally more
759 than 10 thousands of cells analyzed.

760 (D) The RhoA activity dynamics over metaphase measured by FRET analysis in 21 mitotic cells depleting
761 CDC20. All background-subtracted mean FRET intensities were normalized over their corresponding mean
762 FRET intensities at the time points of nuclear envelop breakdown (NEB) or cell adherence (AD) right before
763 rounding up, whichever applied. Cn refers to different cell analyzed. Also see Movie S6.

764 (E) Quantification of CIC structures in cells overexpressing RhoA. Data are mean \pm SD of 4 or more fields with
765 more than 3000 cells analyzed each. $p < 0.001$.

766 (F) Inhibition of CIC formation in CDC20 depleted cells by Y27632, a ROCKs inhibitor that blocks RhoA
767 signaling. Data are mean \pm SD of 4 or more fields with more than 5000 cells analyzed each. $p < 0.0001$.

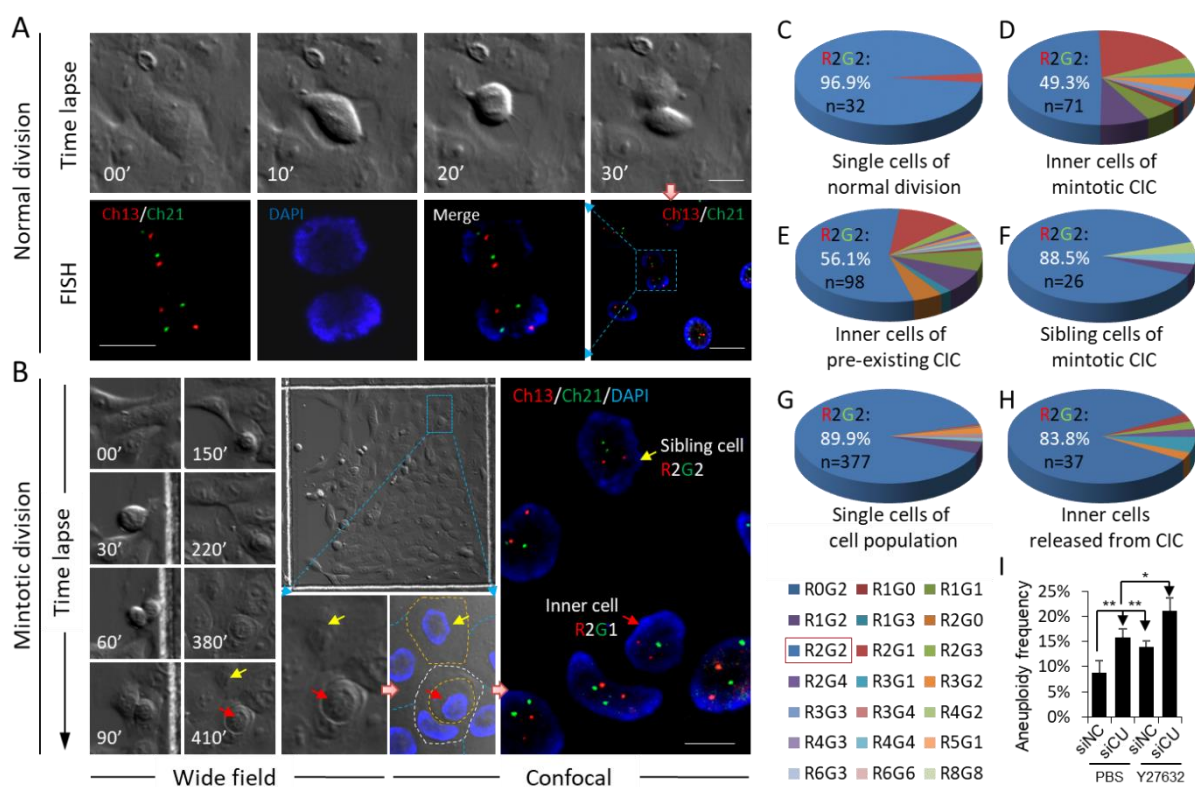
768 (G) Polarized distribution of pMLC at the rear cortex of internalized cell in intermediate CIC structure. Scale
769 bars: 10 μ m. Also see Figure S5E.

770 (H) Rnd3-GFP localizes at the cell-cell junction during CIC formation. Upper graph shows line scan analysis,
771 channeled images were shown underneath. Scale bar: 10 μ m.

772 (I) Rnd3 mRNA level examined by quantitative PCR (qPCR) upon knockdown by RNA interference. Data are
773 mean \pm SD of triplicate experiment. $p < 0.001$.

774 (J) Representative images for junctional localization of pMLC (red) MCF10A cell doublets (right panel) upon
775 Rnd3 depletion (Rnd3 KD), E-cadherin (green) staining indicates cell junctions. Scale bars: 10 μ m.
776 Arrowheads indicate pMLC staining at cell junctions. Also see Figure S5G

777 (K-L) Quantification of entotic (K) and mitotic (L) CIC formation in control (siNC) and Rnd3 (siRnd3) depleted
778 cells. For entotic CIC, data are mean \pm SD of triplicate experiments, n>400 cells for each group; for mitotic
779 CIC, data are mean \pm SD of 4 or more fields with more than 5000 cells analyzed each. $p < 0.01$.



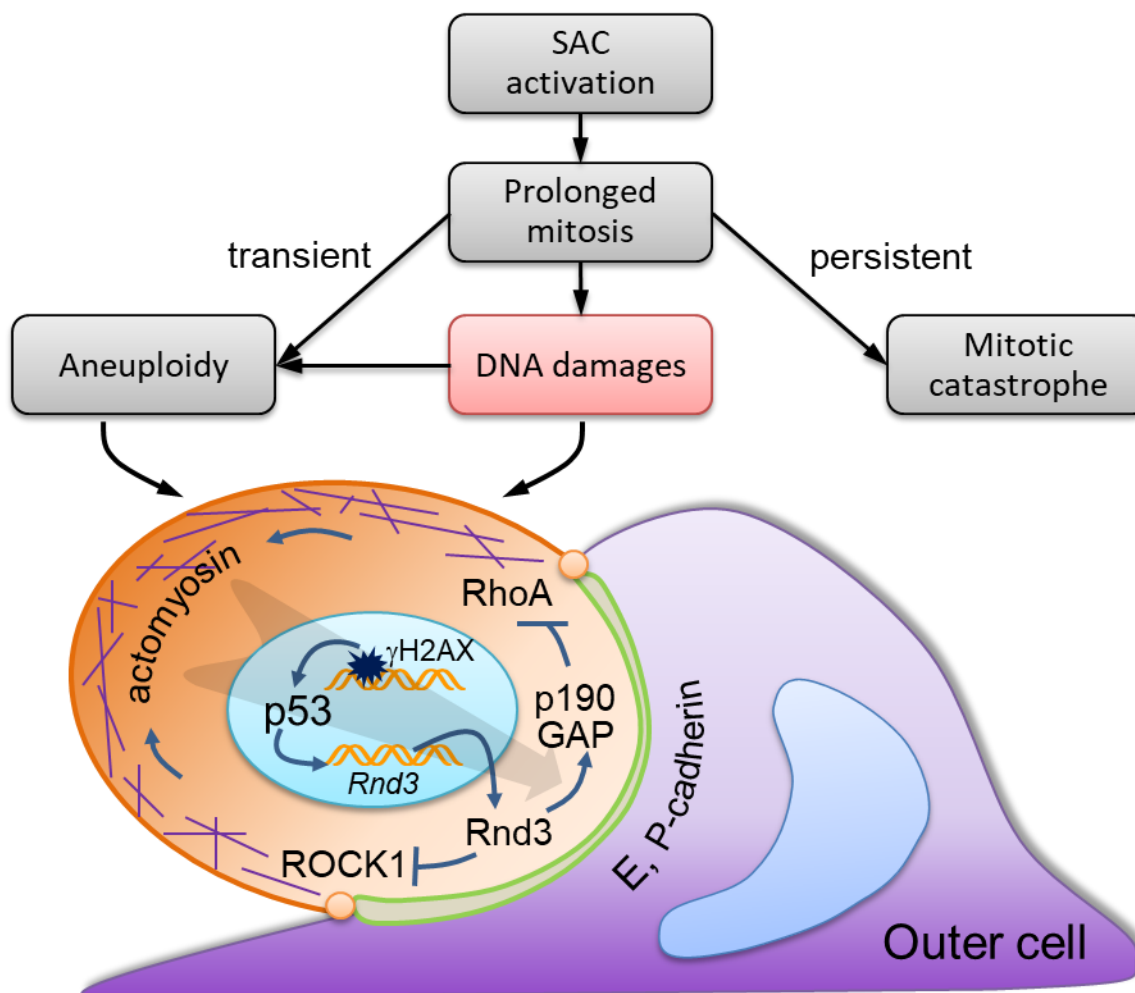
781
782

Figure 6. Mintosis selectively targets non-diploid cells for CIC-mediated death.

- 783 (A) Representative images showing FISH result of normal cell division. Upper panel shows DIC image sequence
784 of time lapse. Lower panel shows FISH results in two daughter cells. Scale bar: 20 μ m for right, 10 μ m for
785 left. Also see Movie S7.
- 786 (B) Representative images showing FISH result of cell division leading to CIC formation. Left panel shows DIC
787 image sequence of time lapse. Middle panel shows the positional information of target cells/structures in
788 gridded glass bottom dish at the end of time lapse imaging. Right panel shows FISH results of selected region
789 in middle panel. Scale bar: 10 μ m. Yellow arrow indicates adherent sibling daughter cell, red arrow indicates
790 daughter cell internalized to form CIC structure. FISH results are presented as RnGn, R for red probe, G for
791 green probe, n for probe number. Also see Movie S7.
- 792 (C-H) Detail quantification and classification of FISH results for daughter cells of normal division with metaphase
793 not more than 30 min (C), daughter cells from cell division that were internalized to form CIC structures (D),
794 inner cells of pre-existing CIC structures of unknown origin (E), daughter cells from cell division that did
795 not form CIC structures (F), single cells of unknown origin in the cell population (G), and internalized cells
796 that were finally released from CIC structure (H), see Figure S9B and Movie S8. FISH results are presented
797 as RnGn, R for red probe, G for green probe, n for probe number. The percentage of R2G2 together with cell
798 number analyzed were shown for each pie picture. The related histories for all cells analyzed were determined
799 by time lapse imaging.
- 800 (I) Quantification of non-diploid cells following mintosis blockade. siNC: non-target control siRNA; siCU:
801 siRNA for CUEDC2. “*” for $p < 0.05$; “**” for $p < 0.01$. For each condition, quantification was performed on
802 >400 cells.
803
804
805

806 **Supplementary Materials**

807



808

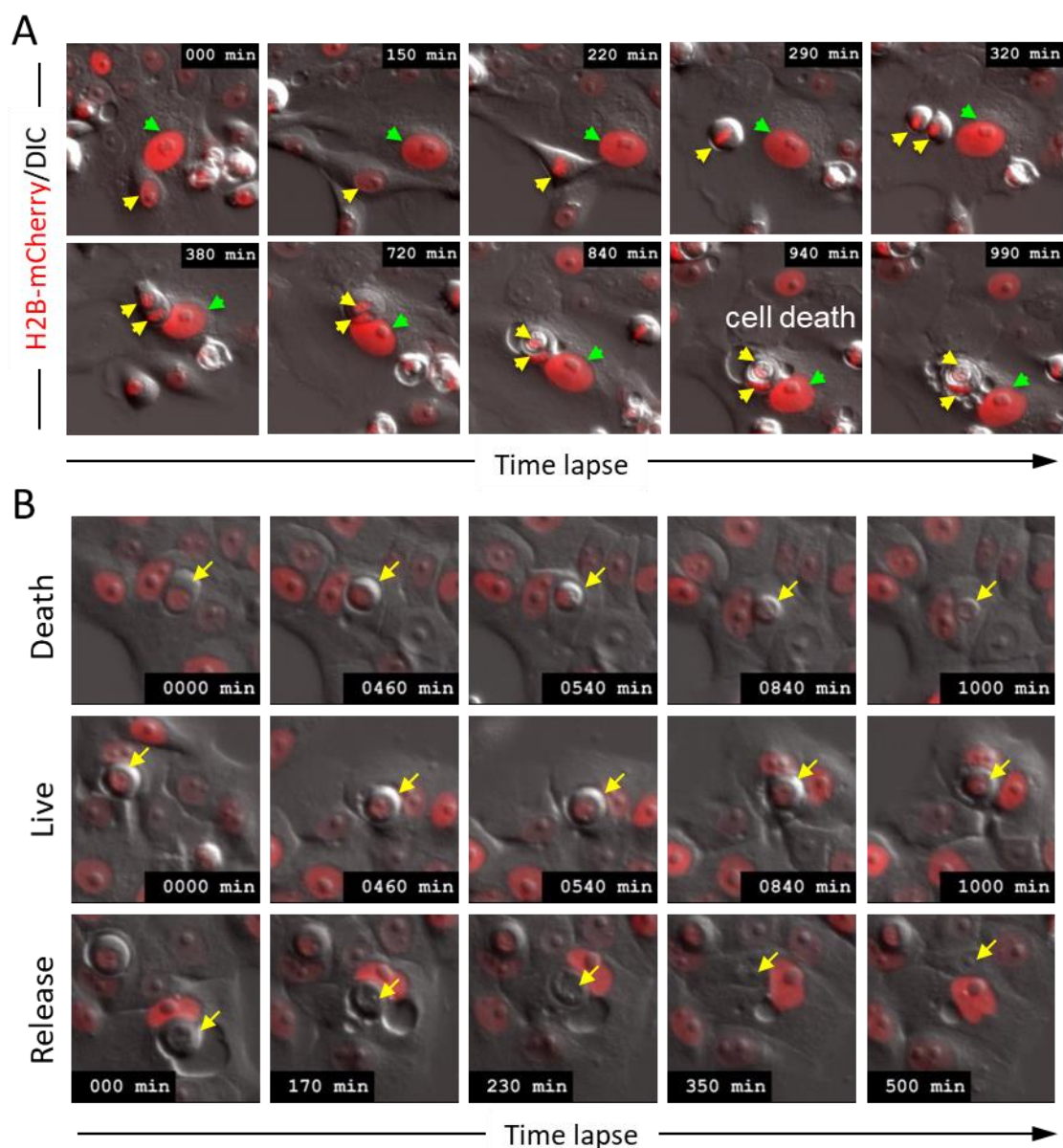
809

810

Figure S1. Working model for p53-dependent postmitotic surveillance by mitosis.

811 SAC activation leads to mitotic arrest characterized by prolonged metaphase. While persistent mitotic arrest
812 activates cell death by mitotic catastrophe prior to cytokinesis, transient mitotic arrest may cause DNA
813 damages that promote chromosome missegregation to give rise to daughter cells of aneuploidy. DNA
814 damages marked by γH2AX activate DDR signaling and p53 in daughter cells. p53 upregulates the expression of
815 downstream target Rnd3 which, by targeting ROCK1 and p190 RhoGAP, inhibits RhoA activities at cell-cell
816 junction where lie E-, P-cadherin, leading to polarized activation of RhoA-actomyosin at rear cortex which
817 drives cell internalization to form CIC structures. Subsequent death promoted by the outer cell eliminates
818 those aneuploid daughter cells to maintain genome integrity.

819



820
821

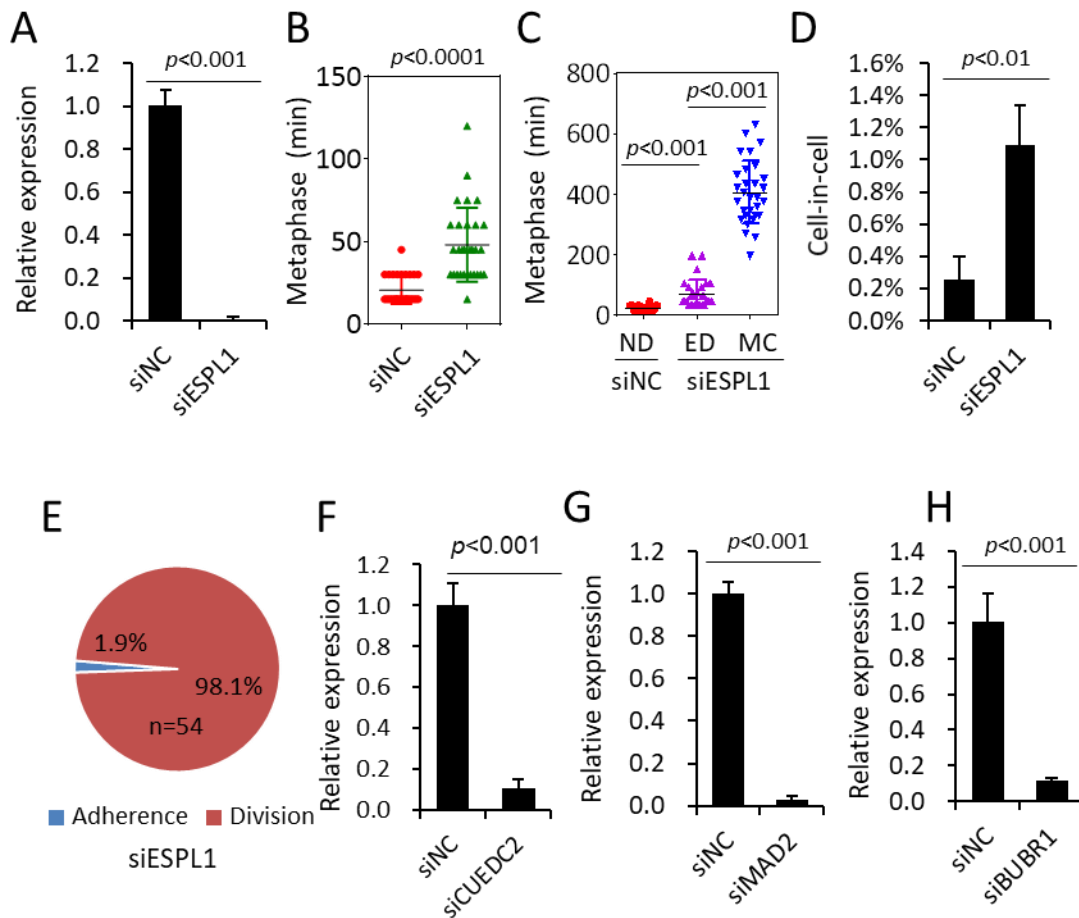
822

Figure S2. Entosis is coupled with mitotic cell division. Related to Figure 1.

823 (A) Image sequence shows the process of entotic cell-in-cell formation and inner cell death following mitotic cell
824 division in MCF10A/H2B-mCherry cells. Yellow arrows indicate cells undergoing mitosis and
825 internalization, green arrows indicate outer cells.

826 (B) Representative image sequences of different inner cell fates for entotic cell-in-cell structures of MCF10A
827 cells. Arrows indicate inner cells. Also see Movie S2.

828



829

830

831

Figure S3. Prolonged mitosis primes cells to undergo entosis. Related to Figure 2.

832 (A) ESPL1 mRNA level examined by quantitative PCR (qPCR) upon knockdown by RNA interference. Data are
833 mean \pm SD of triplicate experiment. $p < 0.001$.

834 (B) Quantification of CIC structures in control (siNC) and ESPL1 (siESPL1) depleted cells. Data are mean \pm SD
835 of 4 or more fields with more than 5000 cells analyzed each. $p < 0.01$.

836 (C) Graph plots metaphase duration of control (siNC, $n=30$) and ESPL1 depleted (siESPL1, $n=30$) cells that
837 didn't undergo entosis or mitotic catastrophe. $p < 0.0001$.

838 (D) Quantification of CIC formation in control (siNC) and ESPL1 depleted (siESPL1) cells. Data are mean \pm SD
839 of 4 or more fields with more than 5000 cells analyzed each. $p < 0.01$.

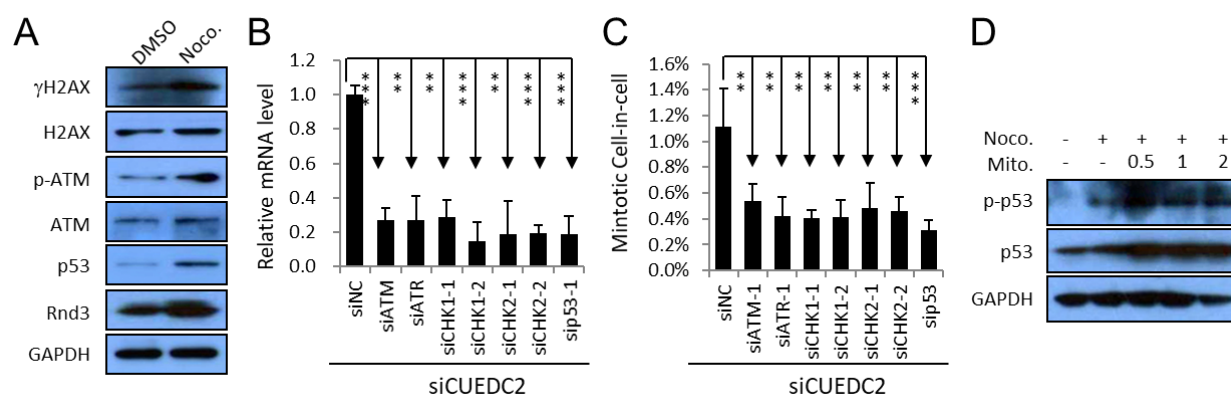
840 (E) Quantification of Entotic Adherence (Adherence) and Entotic Division (Division) in MCF10A cells with
841 ESPL1 depletion.

842 (F) CUEDC2 mRNA level examined by quantitative PCR (qPCR) upon knockdown by RNA interference. Data
843 are mean \pm SD of triplicate experiment. $p < 0.001$.

844 (G) MAD2 mRNA level examined by quantitative PCR (qPCR) upon knockdown by RNA interference. Data are
845 mean \pm SD of triplicate experiment. $p < 0.001$.

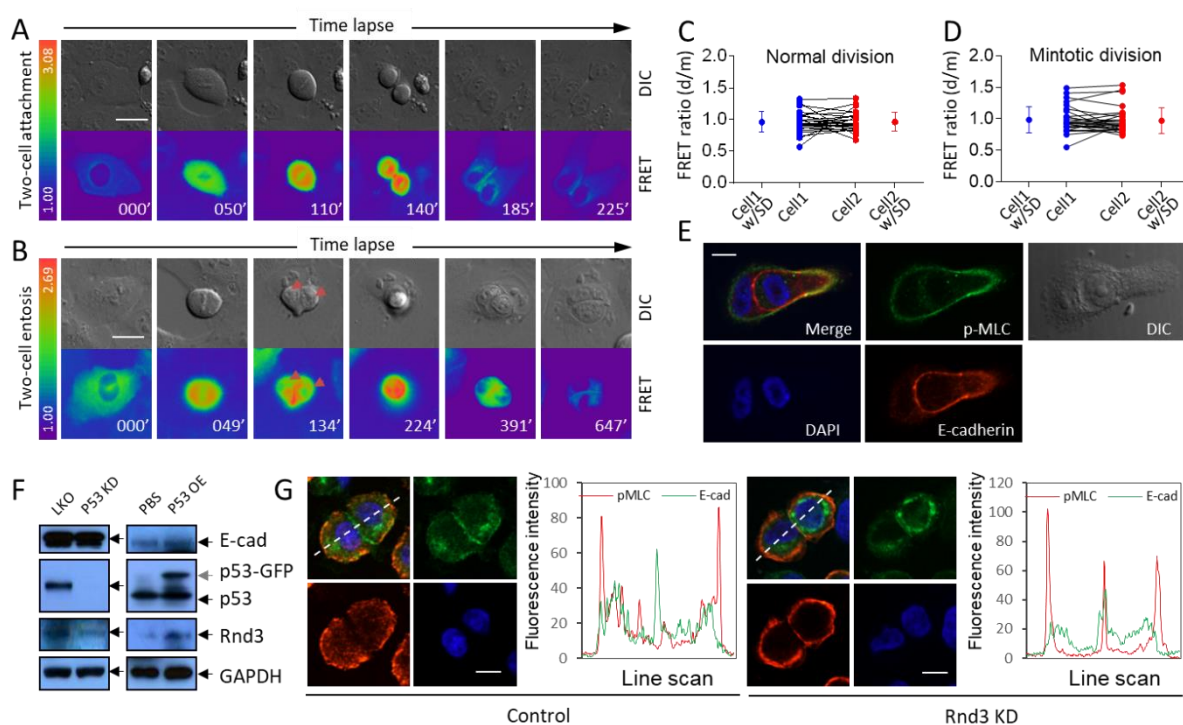
846 (H) BUBR1 mRNA level examined by quantitative PCR (qPCR) upon knockdown by RNA interference. Data
847 are mean \pm SD of triplicate experiment. $p < 0.001$.

848



849
850 **Figure S4. Involvement of DNA damage-p53 pathway in mitosis. Related to Figure 5.**

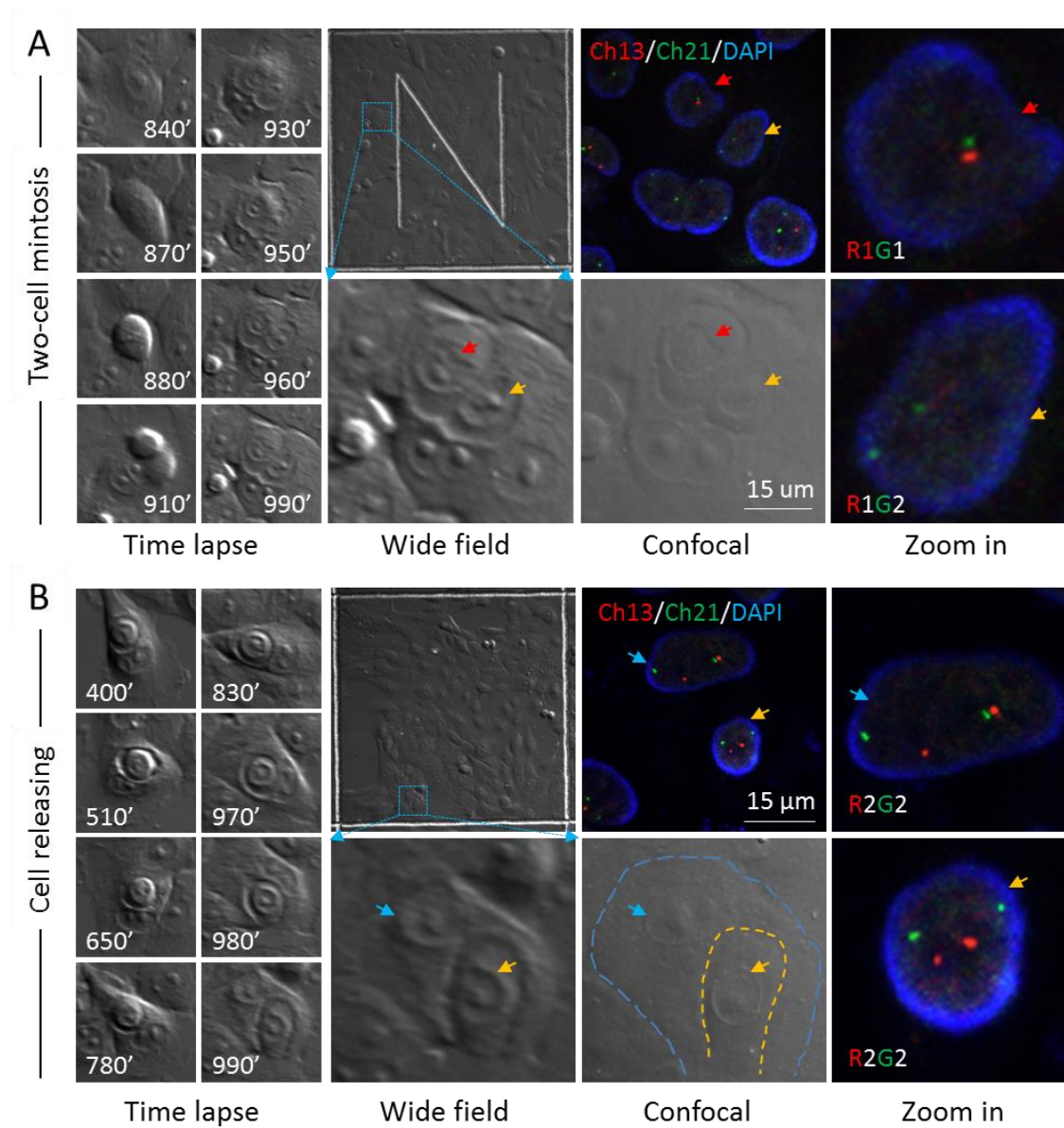
- 851 (A) Activation of DNA damage response (DDR) signaling during mitotic arrest. Expression of genes of DDR
852 pathway in nocodazole (Noco.)-treated MCF10A cells were detected by Western blot.
- 853 (B) mRNA levels of genes in DDR pathway examined by quantitative PCR (qPCR) upon knockdown by RNA
854 interference. Data are mean \pm SD of triplicate experiment. $p < 0.001$.
- 855 (C) Decreased mitotic CIC formation in MCF10A cells upon depletion of genes in DDR pathway by RNA
856 interference. Data are mean \pm SD of 4 or more fields with more than 5000 cells analyzed each. “***” for
857 $p < 0.01$; “****” for $p < 0.001$.
- 858 (D) DNA damages by mitomycin (Mito.) increase expression of p53 and phospho-p53 in cells synchronized in
859 M phase by nocodazole (Noco.).
860



861
862

Figure S5. Compartmentalized RhoA activity by Rnd3 is required for mitosis. Related to Figure 5.

- 863 (A) Representative FRET image sequence shows RhoA activity changes during cell division with two daughter
864 cells attached to plate bottom. Scale bar: 20 μ m.
- 865 (B) Representative FRET image sequence shows RhoA activity changes in cell division with two daughter cells
866 internalized to form CIC structures. Scale bar: 20 μ m.
- 867 (C-D) RhoA FRET ratios between daughter cells right after cytokinesis (d) and their respective mother cells in the
868 end of metaphase (m) in normal cell division (C, n=28) and mitotic cell division (D, n=29).
- 869 (E) Representative images for polarized distribution of pMLC at the rear cortex of internalized cell in
870 intermediate CIC structure. Scale bars: 10 μ m. Identical to Figure 5G.
- 871 (F) Regulation of Rnd3 expression by p53 in MCF10A cells. Left panel shows decreased Rnd3 expression upon
872 stable p53 knockdown (p53 KD) as compared with control (LKO). Right panel shows increased Rnd3
873 expression upon p53-GFP overexpression (p53OE).
- 874 (G) Representative images for junctional localization of pMLC (red) MCF10A cell doublets (right panel) upon
875 Rnd3 depletion (Rnd3 KD), E-cadherin (green) staining indicates cell junctions. Scale bars: 10 μ m.
876 Arrowheads indicate pMLC staining at cell junctions. Related to Figure 5J.
877



878
879

Figure S6. Mitosis selectively targets non-diploid cells for elimination. Related to Figure 6.

- 880 (A) Representative images showing FISH result of cell division leading to internalization of two daughter cells
 881 to form CIC structures. Left panel shows DIC image sequence of time lapse. Middle panel (wide field) shows
 882 the positional information of target cells/structures in gridded glass bottom dish at the end of time lapse
 883 imaging. Right panels (confocal and zoom in) show FISH results of selected region in middle panel. Scale
 884 bar: 15 μm . Yellow and red arrows indicate two daughter cell internalized. FISH results are presented as
 885 RnGn, R for red probe, G for green probe, n for probe number. See Movie S7.
 886 (B) Representative images showing FISH result of cell releasing from CIC structures. Layout is same as that of
 887 (A). Scale bar: 15 μm . Yellow arrow indicates inner cell that is being released. Blue arrow indicates outer
 888 cell. FISH results are presented in the same way as (A). See Movie S7. Related to Figure 6H.
 889

890 **Movie S1. The formation of entotic CIC structures.**

891 **Entotic Adherence:** MCF10A cell indicated by arrows penetrates into one of its neighboring cells
892 to form CIC structure while being adherent to matrix.

893 **Entotic Suspension:** Two MCF10A cells indicated by arrows likely first formed CIC structure
894 while being suspended, and then penetrated into one of their neighboring cells to form CIC
895 structure.

896 **Entotic Division:** Arrow indicated MCF10A cell first underwent cell division with a metaphase of
897 80 min, and then one of the daughter cells internalized into its neighboring cell to form CIC
898 structure.

899 **Normal Division:** Normal cell division with a short metaphase of 20 min and two daughter cells
900 adherent to matrix rapidly.

901

902 **Movie S2. Entosis is coupled with mitotic cell division.**

903 Yellow arrows-indicated cell underwent mitotic cell division, followed by internalization of two
904 daughter cells into their neighboring cell (green arrow). The most inner cell died prior to the end
905 of the time lapse.

906

907 **Movie S3. Inner cell fates in CIC structures.**

908 **Death:** Arrow indicated inner cell of a CIC structure died inside another MCF10A cell.

909 **Unchanged:** Arrow indicated inner cell of a CIC structure stayed alive inside another MCF10A
910 cell to the end of time lapse of 24 h.

911 **Released:** Arrow indicated inner cell initially resided in the vacuole of a CIC structure, then came
912 out alive as indicated by arrows.

913

914 **Movie S4. Catastrophic cell death of mitosis.**

915 CDC20 depleted mitotic MCF10A cell underwent prolonged metaphase of 480 min and finally
916 died in a catastrophic way.

917

918 **Movie S5. Mitosis of different metaphase.**

919 **M=20 min:** Mitotic MCF10A cell underwent short metaphase of 20 min.

920 **M=60 min:** Mitotic MCF10A cell with CDC20 depleted underwent prolonged metaphase of 60
921 min.

922

923 **Movie S6. RhoA activity by FRET during one-cell mitosis.**

924 RhoA activity by FRET in CDC20 depleted MCF10A cell first accumulated during metaphase,
925 then, one of the daughter cells that demonstrated delayed RhoA activity attenuation penetrated
926 into its neighboring cell to form CIC structure, while the daughter cell that rapidly reduced its
927 RhoA activity attached to plate bottom. Left is FRET channel, right is DIC channel.

928

929 **Movie S7. Time lapse for FISH.**

930 **Normal division:** Cell divided with metaphase less than 20 min, two daughter cells attached to
931 plate bottom shortly after division.

932 **Mitotic division:** Cell divided with one of the two daughter cells internalized to form CIC
933 structure at the end of time lapse, while another daughter cell attached to plate bottom shortly after
934 division.

935 **Two-cell mitosis:** Cell divided with both of the two daughter cells internalized to form CIC
936 structure at the end of time lapse.

937 **Inner cell releasing:** The arrow indicated inner cell of a CIC structure started to come out at the
938 end of time lapse.

939